Nonstationarity of a two-dimensional perpendicular shock: Competing mechanisms

Bertrand Lembège, Philippe Savoini, P. Hellinger, P. M. Trávnícek

Nonstationarity of a two-dimensional perpendicular shock: Competing mechanisms

Bertrand Lembège,[1] Philippe Savoini,[1] Petr Hellinger,[2] and Pavel M. Trávníček[2]

Received 18 July 2008; revised 22 October 2008; accepted 28 November 2008; published 26 March 2009.

[1] Two-dimensional particle-in-cell (PIC) simulations are used for analyzing in detail different nonstationary behaviors of a perpendicular supercritical shock. A recent study by Hellinger et al. (2007) has shown that the front of a supercritical shock can be dominated by the emission of large-amplitude whistler waves. These waves inhibit the self-reformation driven by the reflected ions; then, the shock front appears almost "quasi-stationary." The present study stresses new complementary results. First, for a fixed β_i value, the whistler waves emission (WWE) persists for high M_A above a critical Mach number (i.e., $M_A \geq M_A^{\mathrm{WWE}}$). The quasi-stationarity is only apparent and disappears when considering the full 3-D field profiles. Second, for lower M_A, the self-reformation is retrieved and becomes dominant as the amplitude of the whistler waves becomes negligible. Third, there exists a transition regime in M_A within which both processes compete each other. Fourth, these results are observed for a strictly perpendicular shock only as $\mathbf{B}_0$ is within the simulation plane. When $\mathbf{B}_0$ is out of the simulation plane, no whistler waves emission is evidenced and only self-reformation is recovered. Fifth, the occurrence and disappearance of the nonlinear whistler waves are well recovered in both 2-D PIC and 2-D hybrid simulations. The impacts on the results of the mass ratio (2-D PIC simulations), of the resistivity and spatial resolution (2-D hybrid simulations), and of the size of the simulation box along the shock front are analyzed in detail.

Citation: Lembège, B., P. Savoini, P. Hellinger, and P. M. Trávníček (2009), Nonstationarity of a two-dimensional perpendicular shock: Competing mechanisms, *J. Geophys. Res.*, *114*, A03217, doi:10.1029/2008JA013618.

1. Introduction

[2] Previous numerical simulations [*Biskamp and Welter*, 1972; *Quest*, 1985; *Lembège and Dawson*, 1987; *Lembège and Savoini*, 1992; *Hellinger et al.*, 2002] revealed that quasi-perpendicular shocks can be strongly nonstationary in a supercritical regime. One nonstationary mechanism observed in both hybrid and full particle simulations is characterized by a periodic self-reformation of the shock front over ion timescale driven by the accumulation of reflected ions. More precisely, the cyclic period is of the order of an ion gyroperiod calculated from the averaged B field measured in the middle of the ramp (and not from the upstream ion gyroperiod) as measured by *Lembège and Savoini* [1992]. This means that several self-reformations can take place within one upstream ion gyroperiod (commonly, 2–3 for a moderate supercritical shock). In the case of strictly perpendicular shocks, the self-reformation process reveals to be very sensitive to the Alfvén Mach number M_A and the ion upstream β_i [*Hellinger et al.*, 2002; *Hada et al.*, 2003], where β_i is the ratio between the ion kinetic energy and the magnetic field energy. Recent reviews [*Hellinger*, 2003; *Lembège et al.*, 2004] stress the importance of the self-reformation process for the shock properties. One-dimensional (1-D) particle-in-cell (PIC) simulations [*Schmitz et al.*, 2002; *Lee et al.*, 2004] show that the shock reformation leads to a strong energization of a portion of reflected ions during their subsequent interaction with the nonstationary shock. This process has also a strong impact on the formation of energetic electrons (periodic bursts of field-aligned electrons) as shown by *Lembège and Savoini* [2002], with the use of 1-D and 2-D simulations of quasi-perpendicular shocks.

[3] A recent work [*Hellinger et al.*, 2007], called herein Paper 1, based on both 2-D hybrid and 2-D PIC simulations of a strictly perpendicular shock has stressed that large-amplitude coherent whistler waves are emitted in the foot region and dominate the whole shock front dynamics. The main features of these waves are summarized as follows: (1) they appear relatively shortly, at least within a timescale much shorter than one ion gyroperiod; (2) once emitted from the ramp, they are propagating almost at the shock velocity so that they seem "quasi-stationary" with respect to the front, and their frequency in the shock rest frame is zero; (3) their propagation is oblique both to the shock normal and to the static magnetic field direction; (4) their amplitude is maximum within the shock front location; (5) this whistler waves emission is associated with the

[1] CETP, UVSQ, IPSL, CNRS, Velizy, France.
[2] Institute of Atmospheric Physics and Astronomical Institute, AS CR, Prague, Czech Republic.

0148-0227/09/2008JA013618

Table 1. Plasma Parameter Values Used in the 2-D PIC and Hybrid Simulations

		PIC		Hybrid	
Parameter	Description	Electrons	Ions	Electrons	Ions
v_{th}	thermal velocity	0.3	0.012		$0.27/v_A$
λ_D	Debye length	0.42	0.34		
ρ_c	gyroradius	0.84	270		$0.27\ c/\omega_{pi}$
c/ω_p	inertial length	3	60		1
ω_c	gyrofrequency	0.5	0.0012		1
ω_p	plasma frequency	1	0.05		
τ_c	gyroperiod	13	5027		2π
β	kinetic plasma energy/magnetic energy	0.24	0.15	0.24	0.15

disappearance of self-reformation so that this emission inhibits the self-reformation; (6) reflected ions interact with these waves and are strongly diffused within the foot region; and (7) all of these features persist well for certain plasma conditions, i.e., for a supercritical (but still moderate) Mach number regime and/or low β_i. These conditions may be also expressed in terms of $v_{sh}/v_{thi} \gg 1$, similar to the criterion proposed by *Scholer et al.* [2003], where v_{sh} is the shock velocity. In summary, these recent results may seem to be in contradiction with several well-established features of supercritical shocks and raise up three main questions.

[4] 1. The properties of perpendicular shocks in 2-D simulations strongly depend on the orientation of the upstream magnetic field with respect to the simulation plane with two basic cases: $\mathbf{B}_0$ is lying within the simulation plane and $\mathbf{B}_0$ is perpendicular to the simulation plane [*Forslund et al.*, 1984; *Lembège and Savoini*, 1992]. Do these nonlinear whistler waves occur (with inhibition of self-reformation) in both cases?

[5] 2. For the supercritical Mach regime, previous experimental observations at the terrestrial shock evidence a well-defined ion ring in the velocity plane perpendicular to the magnetostatic field [*Sckopke et al.*, 1983] in contrast with scattered ions, as observed in Paper 1. Is the self-reformation of the shock front totally inhibited in all plasma conditions, or can it reappear within some M_A range? If yes, what is this range? Is the range for a Mach number higher than the M_A values considered in Figure 3 of Paper 1 (this figure is reported herein in Figure 1b) or within the transition regime between occurrence/absence of nonlinear whistler waves defined in Figure 1b?

[6] 3. Why have these whistler waves not been observed in previous 2-D PIC and 2-D hybrid simulations?

[7] The purpose of the present work based on several detailed parametric analyses is to answer these questions and to show that the results of Paper 1 were unexpected but are not in disagreement with previous works. Present results show that the relative occurrence of the self-reformation versus the whistler waves emission is strongly dependent on the orientation of the static $\mathbf{B}_0$ field and also on the relative β_i and M_A values. The paper is organized as follows. First, the simulation conditions are summarized in section 2. Second, results of typical 2-D PIC simulations are shown in section 3 as the static $\mathbf{B}_0$ field is within and outside the simulation plane. In addition, a parametric study on the occurrence and the dynamics of whistler waves emission is also detailed as the static $\mathbf{B}_0$ field is within the simulation plane. Results are compared and found to be in a good agreement with those issued from 2-D hybrid simulations. Third, the detailed parametric analysis of section 4 evidences the reasons why present results have not been observed in both previous 2-D PIC and 2-D hybrid simulations. This comparison allows for clarifying that present unexpected results are not in disagreement with previous works but rather stress out that a perpendicular supercritical shock may have different signatures/levels of nonstationarity. Finally, conclusions are drawn in section 5.

2. Simulation Conditions

[8] A 2-D fully electromagnetic particle (PIC) simulation code [*Lembège and Savoini*, 1992] is used where both ions and electrons are treated as individual macroparticles. Different runs have been performed, but the reference run (herein referred to as run 1) is based on the following plasma conditions. The plasma box has 6144×256 grids with a spatial resolution $\Delta = \Delta x = \Delta y = 1/60\ (c/\omega_{pi})$. The number of particles per cell is 4 for each specie, and the time step for the particle advance is $\Delta t = 7.5 \times 10^{-5}\omega_{ci}^{-1}$, where c is the speed of light, ω_{pi} is the upstream ion plasma frequency, and ω_{ci} is the upstream ion cyclotron frequency. The used mass ratio (ion/electron) is $M_i/m_e = 400$. The shock is excited by using a magnetic piston. For strengthening the results obtained with PIC simulations, these will be compared to those obtained by using 2-D hybrid simulations in similar conditions. The ''reference'' 2-D hybrid simulation box is 512×128 points with a spatial resolution $\Delta x = 0.1c/\omega_{pi}$ and $\Delta y = 0.2c/\omega_{pi}$ with 120 particles per cell in the upstream region. Note that the resolution $\Delta x = 0.1c/\omega_{pi}$ is sufficient to resolve the self-reformation process [*Hellinger et al.*, 2002]. The dependence versus the space resolution will be analyzed in more detail in section 4. The time step for the particle advance is $\Delta t = 0.01\omega_{ci}^{-1}$ whereas the magnetic field is advanced with $\Delta t_B = \Delta t/10$. A small resistivity $\eta = 10^{-4}\mu_0 v_A^2 \omega_{ci}^{-1}$ is used; here μ_0 is the magnetic permittivity of vacuum and v_A is the upstream Alfvén velocity. The plasma is streaming along the x axis with $v_0 = 2v_A$ and interacts with a piston (an infinitely conducting wall). In both reference simulations, the $\mathbf{B}_0$ magnetic field is within the simulation plane (aligned along the y axis); the Mach number of the resulting shock is $M_A \sim 4.93$ for the 2-D PIC and $M_A \sim 3.6$ for the 2-D hybrid simulation. The main plasma parameters used in both reference simulation runs are summarized in Table 1.

3. Parametric Analysis

[9] A different parametric analysis will be presented in order to clarify the answers to the questions addressed in this paper and mentioned in section 1.

3.1. Dependence Versus the Orientation of the Static $\mathbf{B}_0$ Field

[10] From the results of Paper 1, one still ignores whether the emitted whistler waves are characteristic of 2-D effects in general or these only require the access to the freedom of propagating obliquely to the shock normal and to the static $\mathbf{B}_0$ field since both effects are mixed. In order to clarify this question, one has to perform two simulations where the static

$\mathbf{B}_0$ field is within (case 1) and outside (case 2) the simulation plane. The labels "case 1" and "case 2" will be used throughout the text both for PIC and hybrid simulations to define the configuration of the $\mathbf{B}_0$ field. In both cases, 2-D effects are fully included, but whistler waves, if emitted, can propagate obliquely to the $\mathbf{B}_0$ field within a wide angular range $(-90°, 90°)$ with respect to the shock normal in case 1 but only perpendicularly to the $\mathbf{B}_0$ field in case 2. Stack plots of the main magnetic field component issued from 2-D PIC simulations are shown in Figure 1. The main result is that self-reformation is fully recovered in case 2 (and associated with the absence of any whistler waves emission), while emission of whistler waves is evidenced (and associated with the absence of self-reformation) in case 1 as in Paper 1. This result stresses the necessity for the nonlinear whistler waves to access to obliquity in order to be emitted from the shock front. Ion reflection (and associated self-reformation) appears to be the dominant process to balance local nonlinear effects (steepening of the shock front) in cases where no access to obliquity is allowed (case 2). Corresponding 3-D plots of the main magnetic field component B_{ty} and B_{tz} and associated y-averaged ion phase space are shown for cases 1 and 2 at a same given time in Figure 2a and 2b. Main differences are evidenced as follows. Shock front rippling clearly appears in case 2 both in the ramp and foot regions (Figure 2a), with a characteristic wavelength much smaller than one ion upstream inertial length c/ω_{pi} (60Δ). The mechanism responsible for this rippling is under active investigation and will be presented in a further paper. In contrast, the wavelength along the shock front is around $2-3c/\omega_{pi}$ for case 1 (presence of nonlinear whistler waves). In addition, it appears clearly (Figure 2b) that reflected ions in case 2 stay relatively well collimated and form a vortex in the ion phase space $v_{xi} - x$, which corresponds to an ion ring in perpendicular velocity space (not shown here). This collimated dynamics forces the reflected ions to accumulate locally at one gyroradius distance from the ramp and to form a foot well separated from this ramp. In such a case, the vortex signature is persistent in time even if reflected ions suffer some diffusion when interacting with the rippled front. This persistent vortex appears to be a necessary condition for initiating and feeding the shock front self-reformation. In contrast, ions are much more diffused in case 1. These differences imply that the diffusion of reflected ions interacting with the front rippling (case 2) is much weaker than that resulting from the interaction of reflected ions with emitted nonlinear whistler waves (case 1) as illustrated in Figure 2b. Two reasons may be invoked: (1) whistler waves are emitted very shortly from the ramp, at least within a time range much smaller than the ion gyroperiod, and (2) the waves amplitude is much larger in case 1 (whistler) than in case 2 (rippling). Additional information is brought with the use of wave energy spectra calculated at a same corresponding time ($t = 8544\omega_{pe}^{-1}$) for each case and shown in Figure 2c. The main results are (1) the whistler wave amplitude (case 1) is much higher than that of the waves responsible for the front rippling (case 2); (2) whistler waves are mainly spreading within the wide foot location (case 1), while waves responsible for the front rippling are rather focused within the narrow ramp (case 2); (3) both types of waves propagate obliquely with respect to the shock front along y, but their propagation angle differs from $\theta_{\mathbf{k},\mathbf{y}} \sim 78°$ (for case 1) to $\theta_{\mathbf{k},\mathbf{y}} \sim 82.8°$ (for case 2); and (4) characteristic wavelengths are totally different with $\lambda = 0.86c/\omega_{pi}$ (case 1) and $\lambda = 0.39c/\omega_{pi}$ (case 2). At least a slight difference is observed between both cases in the M_A regime ($M_A = 4.93$ for case 1, and $M_A = 5$ for case 2) for the same initial conditions. All of these differences affect the conditions of the ion interactions with the waves in each case as it will be shown in a separate study.

[11] In summary, in case 1 (2), whistler waves emission (dissipative effects) is (are) dominant to counteract the nonlinear effects at the shock front (ramp steepening). This difference observed between the two $\mathbf{B}_0$ field configurations suggests that some critical oblique angle may be defined where both processes may balance the ramp steepening in a comparative proportion. The use of a 3-D simulation will be helpful for clarifying this point but is out of the scope of the present paper.

[12] Moreover, results issued from the 2-D hybrid simulation (Figure 3) are very similar to those of 2-D PIC simulations (cases 1 and 2 in Figure 1a). In case 1, nonlinear whistler waves clearly occur; in contrast, whistler waves are totally absent, and self-reformation takes place in case 2. Similarly, some slight differences are observed in the Mach regime between both $\mathbf{B}_0$ field configurations under the same initial conditions ($M_A = 3.6$ in case 1, and $M_A = 3.2$ in case 2). In case 2, no front rippling appears in the shock front in 2-D hybrid simulations, in contrast with 2-D PIC simulations (Figure 2a). This suggests that the waves responsible for the front rippling have a frequency lower than ion frequency; that is, they are not accessible in hybrid simulations. This is in good agreement with previous results in which the rippling waves have been shown to be associated to cross-field currents instabilities in the lower–hybrid frequency range [*Lembège and Savoini*, 1992]. In case 2, one recovers self-reformation in both 2-D PIC and 2-D hybrid simulations. For reference, the self-reformation in the 2-D PIC simulation establishes with a cyclic period $T_{\mathrm{ref}} = 1630\omega_{pe}^{-1}$ comparable to the ion gyroperiod $T_{ci,\mathrm{ramp}} = 1645\omega_{pe}^{-1}$ calculated from the $||\mathbf{B}||$ field measured in middle of the ramp (time-averaged over one reformation cycle). Note that this value differs from the upstream ion gyroperiod since it is only a fraction. Herein, three self-reformations take place within one upstream ion gyroperiod ($T_{ci} = 5027\omega_{pe}^{-1}$). Similar results hold in case 2 for 2-D hybrid simulations ($M_A = 3.2$) with a cyclic period $T_{\mathrm{ref}} = 0.35\tau_{ci}$ comparable to the (ramp-averaged) ion gyroperiod $\tau_{ci,\mathrm{ramp}} = 0.4\tau_{ci}$; in this case, almost 2.5 self-reformations take place within one upstream ion gyroperiod τ_{ci} (not shown herein).

[13] In case 1 of both 2-D hybrid and 2-D PIC simulations, it is important to stress that the absence of self-reformation does not mean that the shock front is strictly stationary (as one could deduce quickly from Figure 1a, for instance). Indeed, a more accurate look at the stack plot of Figure 1 shows that the shock looks quasi-stationary over a large time range covering several upstream ion gyroperiods but, in fact, evidences "nonstationary" signatures over a timescale smaller than one upstream ion gyroperiod. More precisely, some whistler waves emissions (WWE) are reinforced within a pseudocycle as indicated by the arrows in Figure 1a. The time period associated with this pseudocycle is around $T_{\mathrm{WWE}} = 720\omega_{pe}^{-1}$, which is much smaller than the self-reformation period T_{ref} of case 2. This strong time

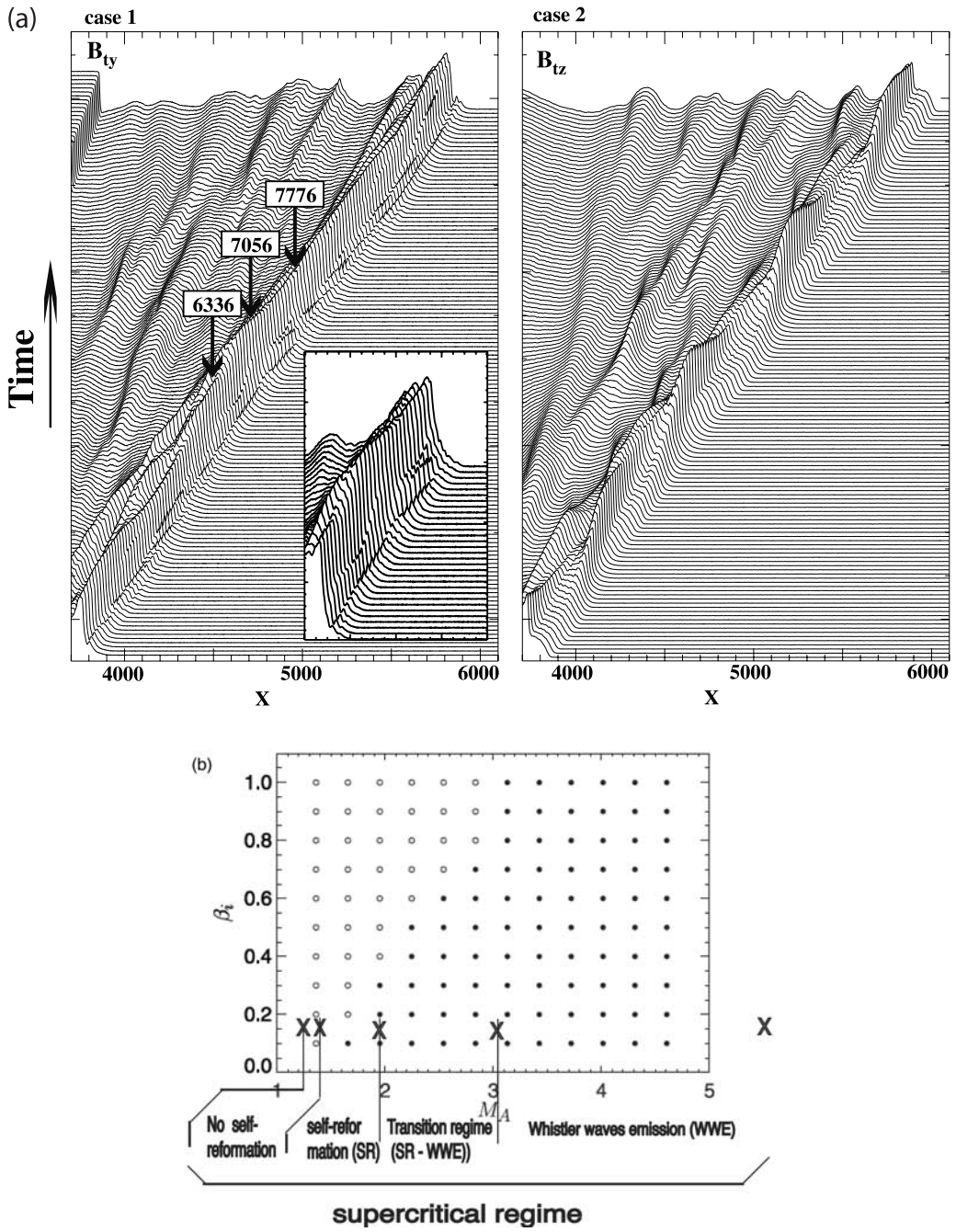

Figure 1. (a) The time stack plot of the y-averaged magnetic field component B_{ty} (case 1) and B_{tz} (case 2), defined as the magnetostatic field, is within ($B_0 = B_{0y}$) and outside ($B_0 = B_{0z}$) the simulation plane. An enlarged view of the stack plot (at late times $4080\omega_{pe}^{-1} \leq t \leq 10368\omega_{pe}^{-1}$, i.e., $5.1\omega_{ci}^{-1} \leq t \leq 12.95\omega_{ci}^{-1}$) is shown herein to evidence more clearly the differences in the shock front dynamics. The time interval between two successive curves is $\Delta t = 48\omega_{pe}^{-1}$. For case 1, the arrows indicate two pseudocycles where the whistler waves emission (WWE) is reinforced; the cyclic period is $T_{\mathrm{WWE}} = 720\omega_{pe}^{-1}$. An enlarged view of the two pseudocycles is inserted. For case 2, the measured time period of shock front self-reformation is $T_{\mathrm{ref}} = 1630\omega_{pe}^{-1}$. (b) The image is extracted from Figure 3 of Paper 1 and is used as a reference throughout the paper. Different supercritical Mach regimes are reported from the results obtained from present 2-D PIC simulations at fixed $\beta_i = 0.15$.

variability of whistler waves emission is better evidenced in three-dimensional plots of the main magnetic component $B_{ty}(x, y)$ as illustrated in Figure 4a. Quite different profiles do not result in each other from a simple time shift but are characterized by emission of larger and/or smaller whistler waves amplitude at different times. This time variability can be analyzed more quantitatively with corresponding energy spectra shown in Figure 4b: (1) the maximum amplitude of

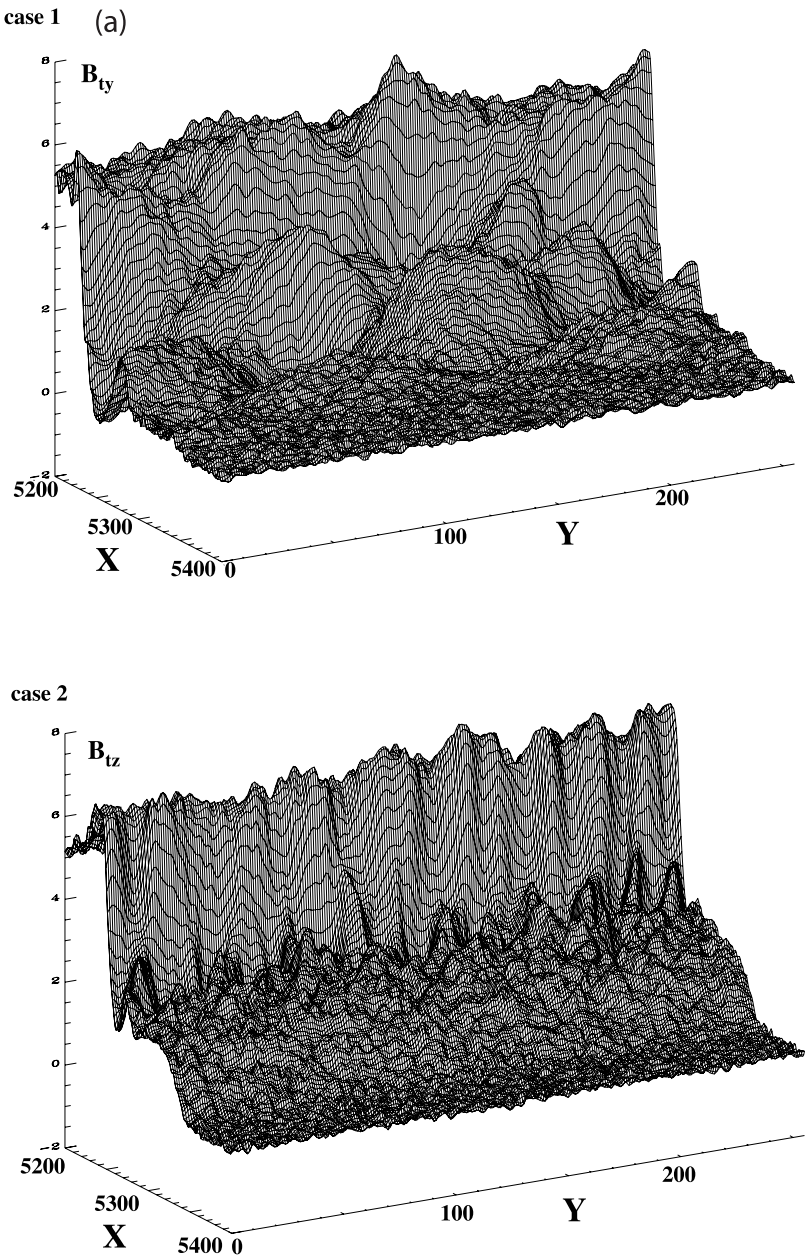

Figure 2. (a) Enlarged three-dimensional view of the main magnetic field component B_{ty} (case 1) and of B_{tz} (case 2) at the same time $t = 8544\omega_{pe}^{-1}$, (b) associated ion phase space, and (c) corresponding power spectra in $k_y - x$ and $k_x - x$ space. In order to evidence more clearly the differences in the ion dynamics between cases 1 and 2, the ion phase space is locally averaged over a limited y interval ($\Delta y = 64\Delta$, where Δ is the unit space grid, between $64 \geq y \geq 128$). For reference, the profile of the corresponding y-averaged main field B_{ty} (case 1) and B_{tz} (case 2) is superimposed in Figure 2b.

the WWE is confirmed to vary strongly (by 1 order of magnitude) within a given cycle mainly along the x axis; (2) at early times of the cycle when the amplitude of WWE is relatively weak, the k_x spectrum is rather wide ($t = 7104\omega_{pe}^{-1}$) but shrinks and concentrates to lower k as time increases, which means that whistler waves are emitted along x with quite different wavelengths at early times; (3) the direction of the WWE is also strongly varying from $\theta_{\mathbf{k},\mathbf{B}} \sim 81.8°$ to $\theta_{\mathbf{k},\mathbf{B}} \sim 63.8°$ from $t = 7104\omega_{pe}^{-1}$ to $t = 7680\omega_{pe}^{-1}$, respectively; and (4) the associated wavelength varies from $\lambda = 0.57c/\omega_{pi}$ to $\lambda = 1.02c/\omega_{pi}$ from $t = 7104\omega_{pe}^{-1}$ to $t = 7680\omega_{pe}^{-1}$, respectively. All the differences may have a strong impact on the ion-whistler interactions which will be analyzed separately.

[14] This pseudocycle may be expressed in terms of successive steps of ''under strengthening'' and ''over strengthening'' of the ramp steepening. During the under-strengthening stage, nonlinear whistler waves are emitted with amplitude comparable to the ramp (Figure 4a). During this stage, wave energy is evacuated from the ramp to the upstream region and the local ramp steepening becomes weaker. In addition, these emitted whistler waves interact

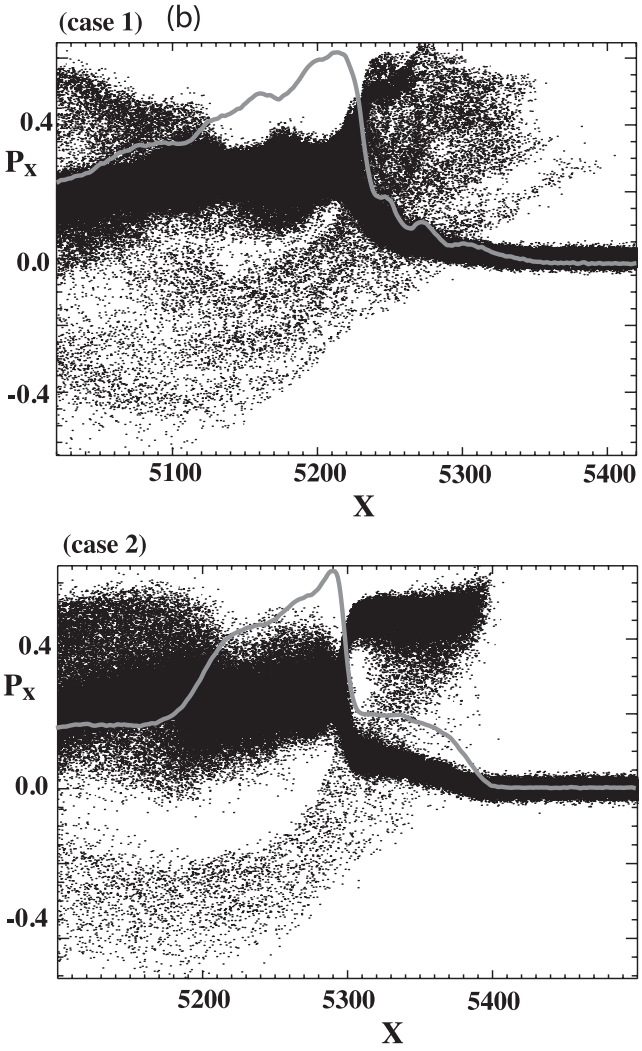

Figure 2. (continued)

with reflected ions. Then, two types of local dissipation effects take place within the front: (1) ions which are reflected (by the macroscopic **E** and **B** fields) at the front and (2) reflected ions which interact with the nonlinear whistler waves. No noticeable interaction of incoming ions with these whistler waves is evidenced (Figure 2b, case 1); these only suffer some local compression. During the second interaction, some wave damping takes place and the local emitted wave steepening reduces. Their (y-averaged) oscillatory signature is less evidenced as illustrated within one pseudoperiod $7056\omega_{pe}^{-1} \leq t \leq 7776\omega_{pe}^{-1}$ in Figure 1a. Ramp and foot regions are more difficult to separate clearly, and the whole shock front looks smoother (as at time $t = 7776\omega_{pe}^{-1}$ in Figure 1a). New incoming ions are less predecelerated in the foot region before reaching the ramp. As a consequence, the ramp can recover a stronger steepening in the so-called over-strengthening stage. When large enough, this steepening can reinitiate a new pseudocycle of reinforced whistler waves emission. The label "pseudo" is used in order to express that whistler waves emission never stops, but only the wave amplitude is more or less amplified versus time. For reference, we identify the beginning of each pseudocycle in Figure 1a at the times when the modulations in the foot of the y-integrated B_{ty} profile are the smoothest (weakest amplitude).

3.2. Dependence Versus the Mach Regime as the B_0 Field is Within the Simulation Plane

[15] Figure 1b clearly shows that nonlinear whistler waves are emitted from the ramp in certain plasma and shock conditions, namely, for a relatively low β_i/high Mach number M_A. Such conditions are equivalent to considering high values of the ratio v_{sh}/v_{thi} ($\gg$1), where v_{sh} and v_{thi} are the shock velocity and the upstream ion thermal velocity, respectively. In these conditions, this emission is the dominant effect and inhibits the self-reformation which disappears in both 2-D hybrid and 2-D PIC simulations. However, these (β_i and M_A) conditions are similar to those for which self-reformation appears in 1-D hybrid simulation. Then, one can wonder whether the self-reformation of the shock front can reappear or not for a much higher Mach number and/or in the transition regime (between the occurrence and absence of self-reformation in 1-D hybrid simulations), i.e., for lower M_A as shown in Figure 1b. For clarity, we will separate the analysis of the results obtained for 2-D PIC and 2-D hybrid simulations.

3.2.1. Impact of M_A Variation in 2-D PIC Simulations

[16] In order to clarify the impact of M_A variation, we have performed a parametric analysis with 2-D PIC simulations by varying Mach number M_A for a fixed β_i value, starting from the reference run (M_A = 4.93) of Figure 1a (case 1). Stack plots of the main magnetic field B_{ty} are plotted in Figure 5 for four typical cases (M_A = 8.2, 2.54, 1.9, and 1.7). Several striking features appear.

[17] 1. The emission of nonlinear whistler waves disappears simultaneously as the self-reformation reappears as M_A decreases below a certain threshold named M_A^{WWE}. More exactly, there is an M_A value interval around M_A^{WWE} within which both signatures of self-reformation and nonlinear whistler waves emission occur and are mixed. This range (herein $1.95 \leq M_A \leq 3.05$) allows for refining Figure 3 of Paper 1. A characteristic feature of this range is that a few self-reformations are quite visible at early times of the run (not shown) and are partially suppressed in time as the whistler waves amplitude grows and reaches a certain amplitude to diffuse the reflected ions. However, this amplitude is not high enough to control totally the shock front dynamics, and both processes can coexist together. This range indicates that a smooth transition exists between both regimes instead of an abrupt transition as in Paper 1.

[18] 2. This self-reformation even persists for quite low M_A values, which indicates that a still noticeable percentage of ions are reflected to feed it.

[19] 3. In contrast, a much higher M_A regime only exhibits nonlinear whistler emission and no self-reformation is observed at any times of the run. These features, which are observed for the first time to the knowledge of the authors, have several impacts.

[20] Present results clearly evidence the existence of several critical Mach number regimes whose features are summarized in Figure 1b. These complete in a simple approach (i.e., one β_i value is considered herein), the general view reached at present time on 2-D perpendicular shocks dynamics; indeed, running 2-D PIC simulations for

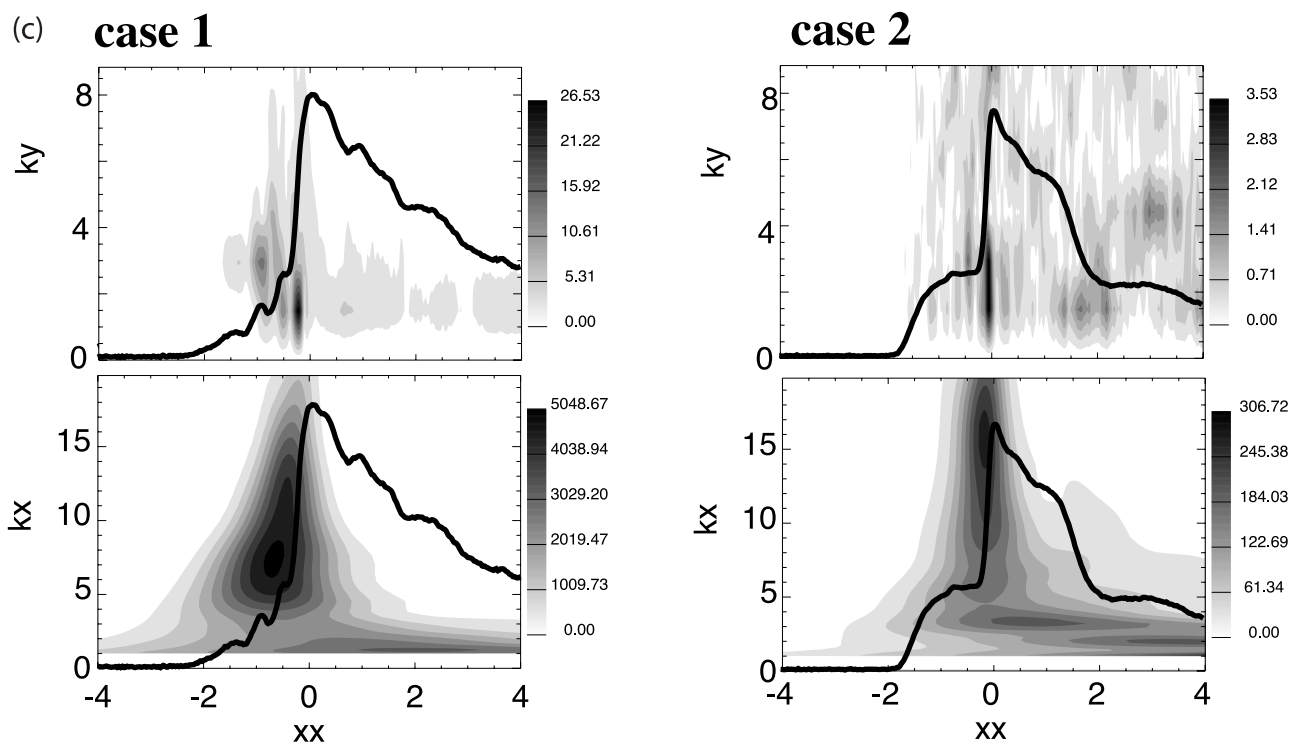

Figure 2. (continued)

both varying different β_i and M_A values are quite expensive. It is well known that for very low M_A (subcritical regime), almost no ions are reflected; their density is too low to raise up a clear foot signature in front of the ramp. The dissipation brought by the resistivity alone is large enough to balance the ramp steepening. As M_A increases above a first critical threshold value M_A*, a certain percentage of ions are reflected. These reflected ions bring the necessary dissipation (in addition to the resistivity) to compensate the stronger ramp steepening. However, reflected ions are responsible for the foot formation (characteristic of the supercritical shock regime), but their percentage is still not strong enough to initiate the self-reformation (herein $1.25 \leq M_A \leq 1.4$). Results issued from an extensive parametric study (not detailed) stress that, as M_A still keeps increasing above a second critical threshold M_A^{SR}, the percentage of reflected ions becomes large enough to initiate the self-reformation process (SR) over a foot (0.3048 m) distance from the ramp. The transition between stationary and nonstationary shock front (self-reformation) takes place around $M_A^{SR} = 1.4$. The present study shows that as M_A still increases above a third critical threshold M_A^{WWE} (more exactly, through a transition regime $1.95 \leq M_A \leq 3.05$ in Figure 1b), the dissipation brought by the reflected ions is not strong enough anymore to balance the stronger ramp steepening. At such a high Mach number, no additional form of dissipation is available anymore. The only available processes able to compensate such a high ramp steepening arise herein via the emission of large-amplitude whistler waves. Whether WWE is due to nonlinear dispersive process is still a topic of debate. Indeed, in a linear regime, such dispersive effects are not allowed to propagate perpendicular to the static magnetic field, and nonlinear dispersive effects may be invoked. This overall scenario seems to be in favor of wave decay processes taking place in the ramp to explain the emission of nonlinear whistler waves as suggested in Paper 1. However, a rigorous theoretical evidence of this process has not been made yet and is still necessary. Above this threshold M_A^{WWE}, the wave energy accumulated in the shock ramp (because of the steepening) is so large that a wave decay is initiated and a mother wave gives birth to two daughter waves propagating symmetrically with respect to the shock normal as suggested in Paper 1. The nonlinear behavior is illustrated herein by the fact that emitted waves reach an amplitude comparable to that of the ramp (Figure 2a) and persist quite well for M_A much above M_A^{WWE} (Figure 6a). This process allows for evacuating extra energy of waves from the ramp. It is important to stress that this whole scenario stands only for case 1 where the static field $\mathbf{B}_0$ is within the simulation plane.

[21] A deeper analysis of Figure 5 evidences that the number of pseudocycles associated with a reinforcement of the whistler waves emission is increasing with higher M_A above the threshold M_A^{WWE} (Figures 1a and 5). As M_A decreases through the transition regime (herein $1.95 \leq M_A \leq 3.05$), these pseudocycles may persist but are embedded within the larger period cycle of self-reformation which becomes more evident (Figures 5b–5c) and progressively disappears as the self-reformation signature becomes dominant for lower M_A as in Figure 5d. This embedding effect is more evidenced in three-dimensional views of the main magnetic field component B_{ty} plotted for decreasing values of the Mach number at a same chosen time

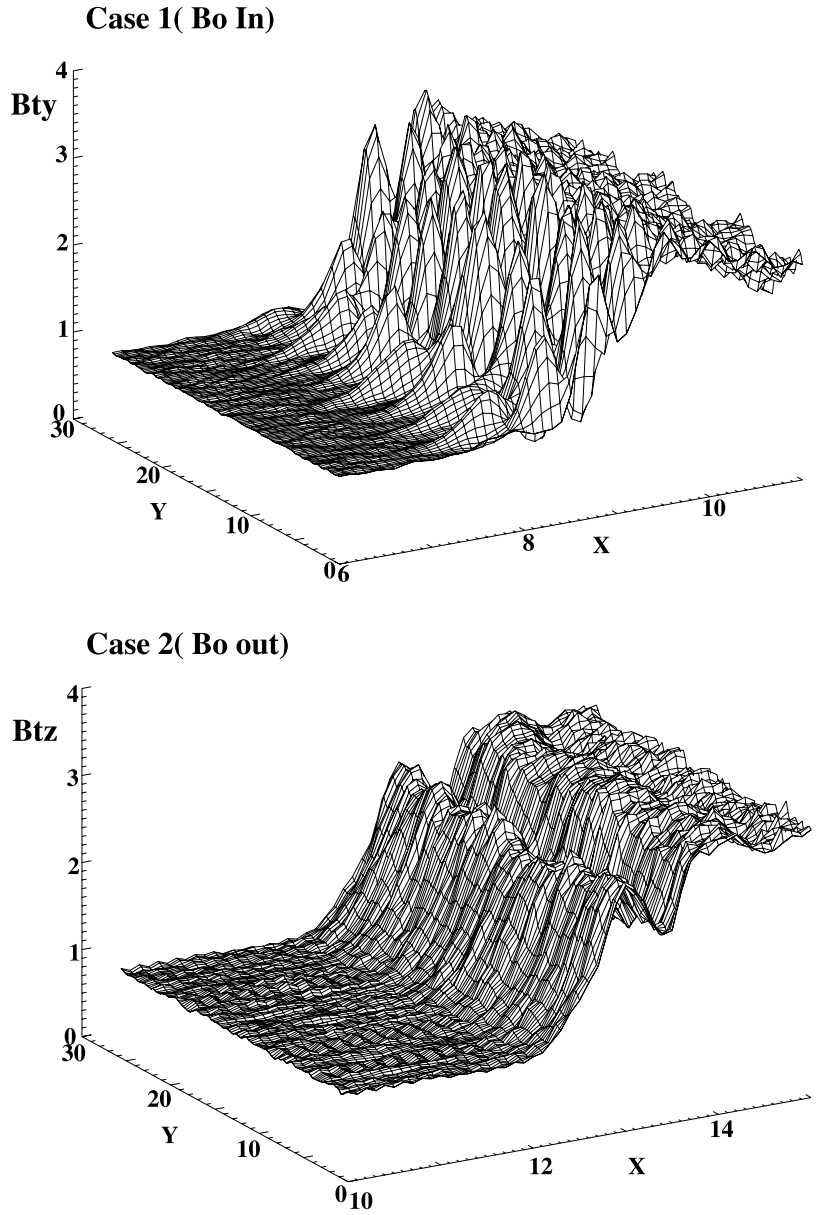

Figure 3. Enlarged three-dimensional view of the main magnetic field component B_{ty} (case 1, with M_A = 3.6) and B_{tz} (case 2, with M_A = 3.2) issued from 2-D hybrid simulations at the same time (t = $28\omega_{ci}^{-1}$) with resistivity $\eta = 10^{-4}\mu_0 v_A^2 \omega_{ci}^{-1}$ and space resolution $\Delta x = 0.1c/\omega_{pi}$ and $\Delta y = 0.2c/\omega_{pi}$.

(Figure 6). For high M_A (8.2), the amplitude of the whistler waves is comparable to that of the ramp (Figure 6a). As M_A decreases, the wave amplitude progressively decreases, and a (relatively) more homogeneous shock front is progressively evidenced. For lower M_A, one recovers a clearer ramp (Figure 6d); however, the foot region is still polluted by some (lower-amplitude) wave activity and suffers a strong modulation along the shock front. The occurrence of the self-reformation process may be more clearly evidenced by analyzing the corresponding ion phase space plots shown in Figure 7 for the same corresponding times and Mach regimes as in Figure 6. A same spatial range (Δx = 500) has been used for clarifying the differences in the foot extension within the upstream region between the different regimes. For large M_A (above M_A^{WWE}), the ion diffusion is strong as ions strongly interact with large-amplitude whistler waves (Figure 7a). This diffusion takes place in both velocity and real space. As M_A decreases, the diffusion is less efficient since reflected ions interact with lower-amplitude whistler waves. As a consequence, their collimated motion expected during their reflection (as long as condition $v_{sh}/v_{thi} \gg 1$ is satisfied) becomes progressively more apparent; a vortex signature appears more clearly in the ion phase space, which is a necessary condition for initiating and feeding the self-reformation process. Figures 7b–7c illustrate the competition between the two processes. For lower M_A, the diffusion is too weak with respect to the collimated motion of reflected ions; a clear vortex is evidenced in the ion phase space (Figures 7c–7d), and the self-reformation becomes dominant (Figures 5c–5d).

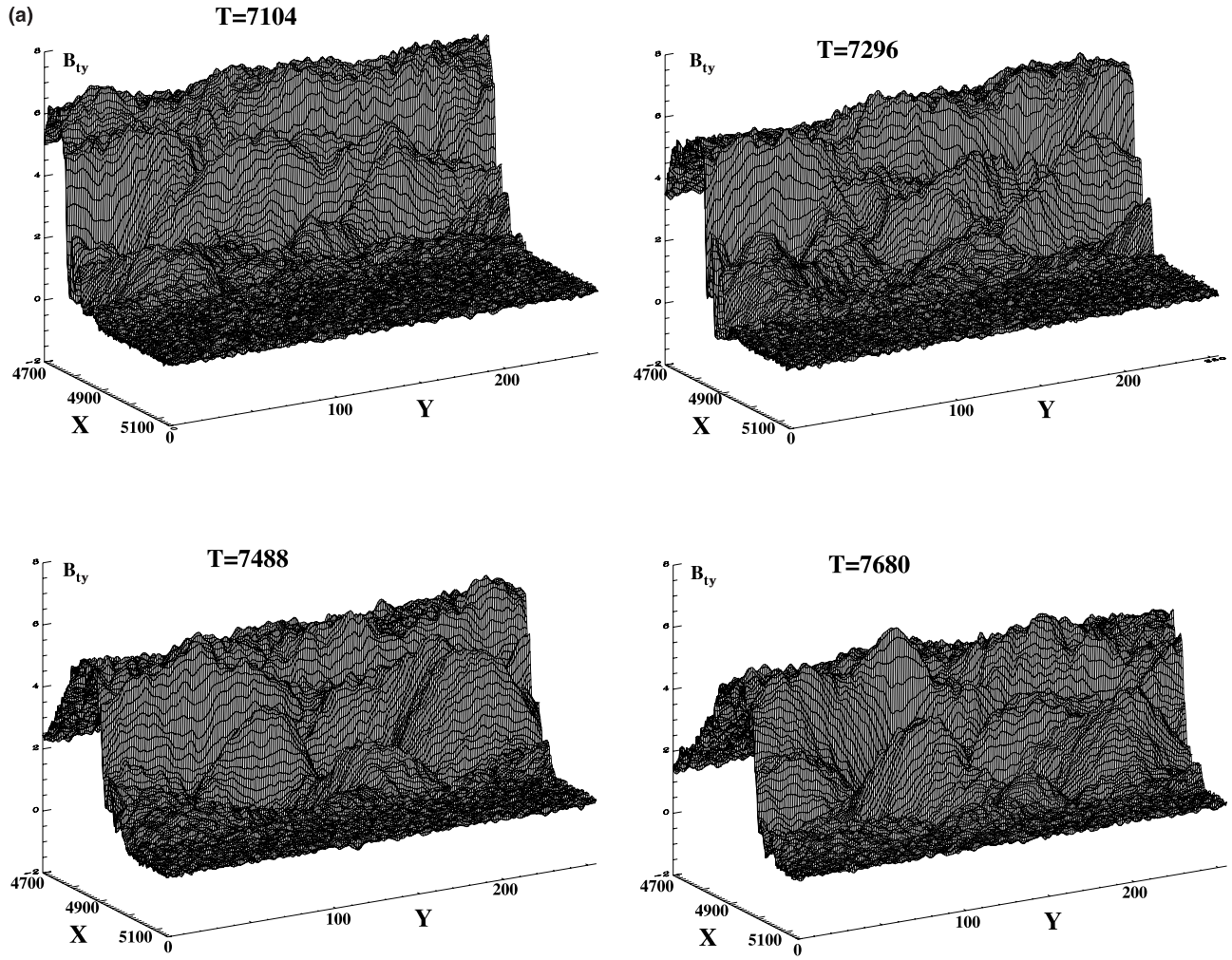

Figure 4. (a) Enlarged three-dimensional view of the y-averaged magnetic field component B_{ty} (case 1) at four different times t = 7104, 7296, 7488, and $7680\omega_{pe}^{-1}$ within a pseudoperiod of shock front variability ($7056 \leq t \leq 7776$). This time range is indicated by arrows in Figure 1a (case 1). (b) Wave energy power spectra corresponding to early and late times (t = 7104 and $7680\omega_{pe}^{-1}$) of the pseudocycle. Results are issued from 2-D PIC simulation.

3.2.2. Impact of M_A Variation in 2-D Hybrid Simulations

[22] In order to reinforce present results, a similar parametric analysis has been performed with 2-D hybrid simulations and compared to 2-D PIC simulations. As detailed in section 4, this comparison requires a certain care since hybrid simulation results are strongly dependant on both the resistivity and the space resolution values. One key point is that the occurrence and absence of nonlinear whistler waves are well evidenced (Figure 1b) and in good agreement in both types of simulation. However, some differences between 2-D PIC and 2-D hybrid simulation results occur within the transition regime and in the evidence of self-reformation signatures at low (still supercritical) M_A.

[23] 1. An extensive parametric analysis has been performed with 2-D hybrid runs (less expensive than 2-D PIC runs) in which the B_{ty} amplitude of the nonlinear whistler waves has been measured versus the Mach number M_A for a same fixed β_i value (case 1). The wave amplitude has been measured by subtracting the y-averaged 1-D profile of B_{ty} from the full 2-D B_{ty} (which allows for eliminating any wave effects along the y direction). Figure 8 shows the energy of these whistler waves measured for different M_A values; each point corresponds to a given 2-D hybrid simulation run. Two sets of results have been obtained for two different spatial resolutions: $\Delta x = 0.1c/\omega_{pi}$ (Figure 8a) and $\Delta x = 0.05c/\omega_{pi}$ (Figure 8b). Let us consider the case $\Delta x = 0.1c/\omega_{pi}$ where clearly three characteristic M_A regimes may be defined where both processes compete with each other to balance the ramp steepening: (1) for weak M_A ($\leq$1.84), the whistler waves amplitude is negligible and almost no waves are detected; in this regime, dissipative effects brought by reflected ions are dominant; (2) for $1.84 \leq M_A \leq 2$, the whistler waves amplitude increases with M_A, which indicates that dissipative effects alone (brought mainly by reflected ions) are not strong enough, and additional nonlinear whistler waves are emitted to compensate this lack of balance; and (3) for $M_A \geq 2$, first, the wave amplitude is almost constant as M_A increases which suggests that both dissipative effects (reflected ions) and waves emission participate to the

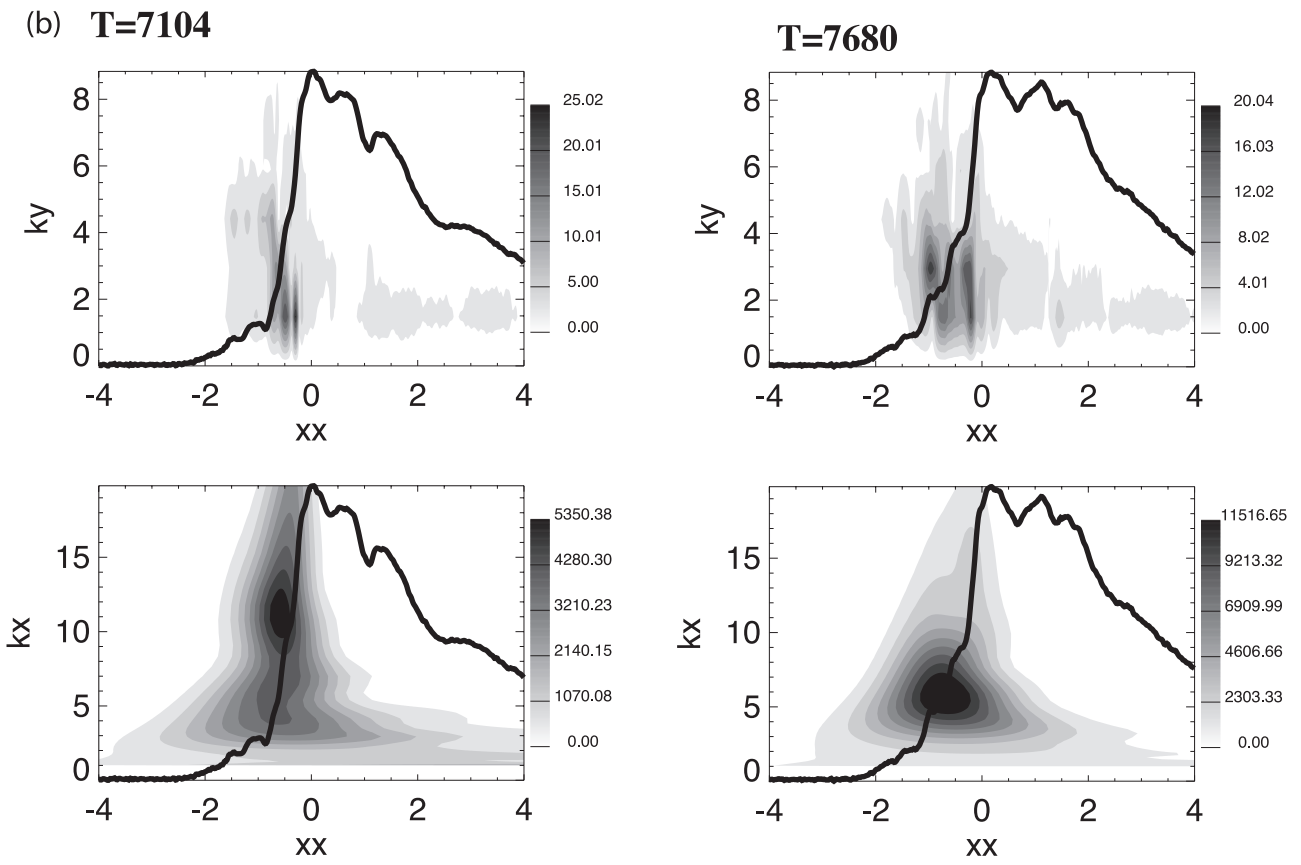

Figure 4. (continued)

balance in comparative proportion, but for higher M_A, the B_{ty} amplitude increases drastically; dissipative effects are saturating, and the waves emission is the main dominant process balancing the strong increase of the ramp steepening. Then, one can identify the range $1.84 \leq M_A \leq 2$ as the transition regime for hybrid simulations. One expects that the use of a higher resolution ($\Delta x = 0.05c/\omega_{pi}$) allows the access to a stronger steepening and then to better conditions for comparing with 2-D PIC simulation results. Figure 8b shows that (1) the general features of Figure 8a are still maintained when using a higher resolution; (2) the corresponding transition regime is larger ($1.55 \leq M_A \leq 2$ instead of $1.84 \leq M_A \leq 2$) and extends to a lower M_A value; (3) the minimum value $M_A = 1.55$ of the interval is approaching the M_A value where the self-reformation restarts for 2-D PIC simulation ($M_A = 1.4$ in Figure 1b); (4) within this transition regime, the amplitude of the emitted whistler waves is lower, and (5) around $M_A = 2$, a certain jump is observed in the emitted waves amplitude; this jump fits well with the beginning of the transition regime observed in 2-D PIC simulations ($M_A = 1.95$ in Figure 1b).

[24] 2. The next step consists in verifying whether the disappearance of nonlinear whistler waves is still correlated with the occurrence of the self-reformation as M_A decreases as evidenced for 2-D PIC simulations (Figure 5). Present results show that this is not the case: no clear and persistent self-reformation has been retrieved in 2-D hybrid results for comparative (low-) M_A regimes, whatever the used space resolution is ($\Delta x = 0.1$ or $0.05c/\omega_{pi}$). Results are illustrated in Figure 9 for different Mach regimes and for the same $\Delta x = 0.05c/\omega_{pi}$. A deeper investigation evidences that both processes are present in the same run, but their coexistence differs from that observed for 2-D PIC simulations. More precisely, for weak M_A (1.49), the y-averaged shock front looks like stationary at any time of the run (Figure 9a) since not enough incoming ions are reflected to feed the self-reformation and the amplitude of the emitted whistler waves is almost negligible (Figure 8b). For higher M_A (1.92) within the transition regime defined in Figure 8b, the self-reformation starts first early in the run simultaneously as the whistler waves amplitude slowly grows (Figure 9b). As time evolves, the waves amplitude reaches a level high enough to largely diffuse the reflected ions which inhibits the self-reformation. The coexistence of the two processes in the same run is more sequential than simultaneous (as for 2-D PIC simulations). This conflict is clearly apparent around time $t = 4\text{–}5\omega_{ci}^{-1}$ (indicated by an arrow in Figure 9b) after which the y-averaged signature of the whistler waves is dominant. Indeed, at that time the emitted whistler waves reach a relatively large amplitude $B_{ty}/B_0 = 0.2$, which is a good quantitative indicator of the wave threshold for the transition between the two processes. As M_A keeps increasing, the self-reformation still starts first (Figure 9c) or totally disappears even at an early time (Figure 9d), while the emitted whistler waves reach a higher amplitude at later times. For higher M_A (Figure 9d), the large-amplitude whistler waves emission is accompanied by some pseudo-cycles (where the whistler waves are periodically strengthened) similar to those observed in 2-D PIC simulations (Figure 5). In summary, for 2-D hybrid simulations, a decrease of M_A is characterized by the progressive disappearance of the whistler waves emission only; no time

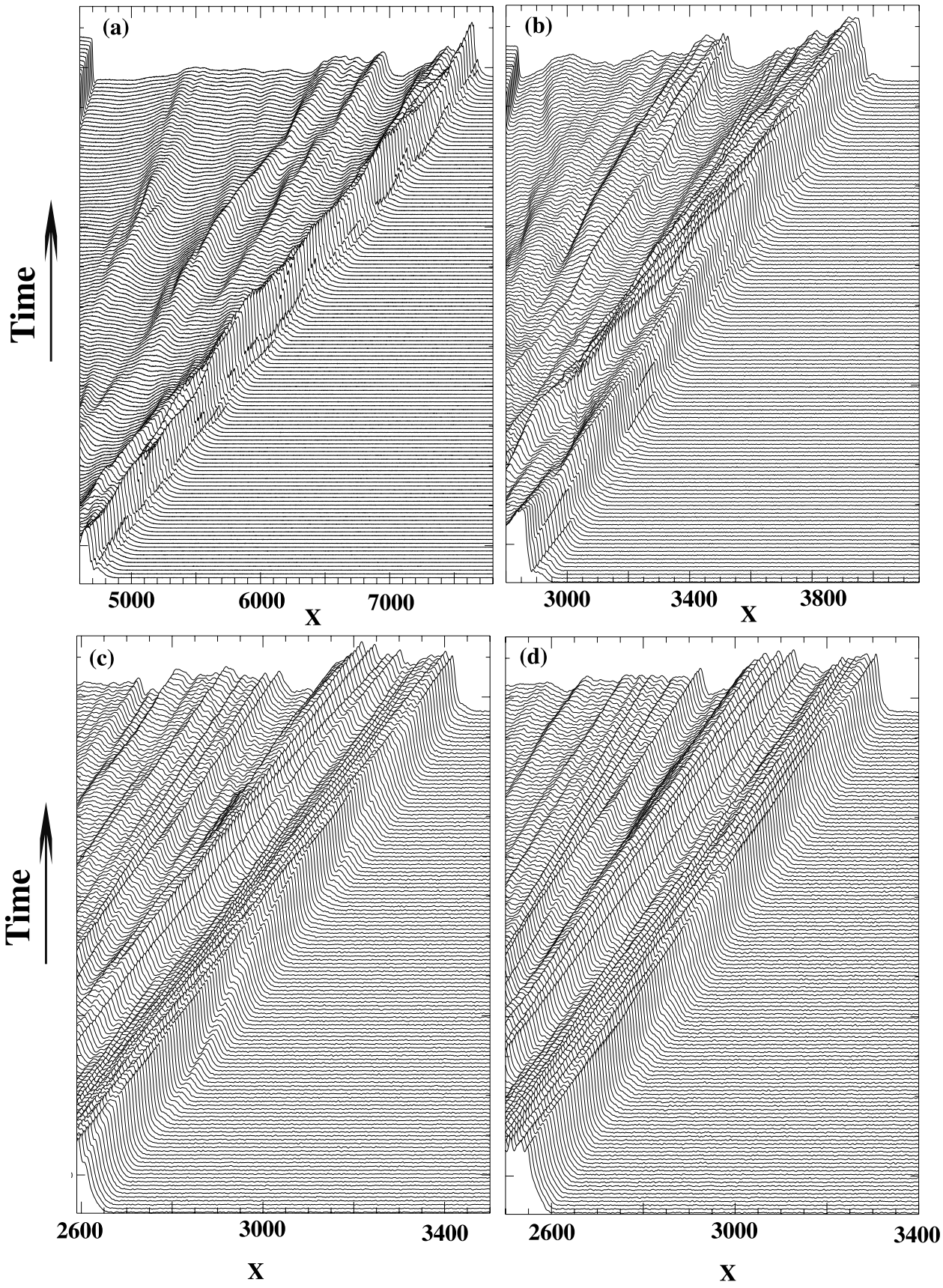

Figure 5. Stack plots of the y-averaged magnetic field B_y (case 1) for (a) $M_A = 8.2$, (b) $M_A = 2.54$, (c) $M_A = 1.9$, and (d) $M_A = 1.7$ for the same time interval ($5.1\omega_{ci}^{-1} \leq t \leq 12.95\omega_{ci}^{-1}$) as for Figure 1. Results issued from 2-D PIC simulation.

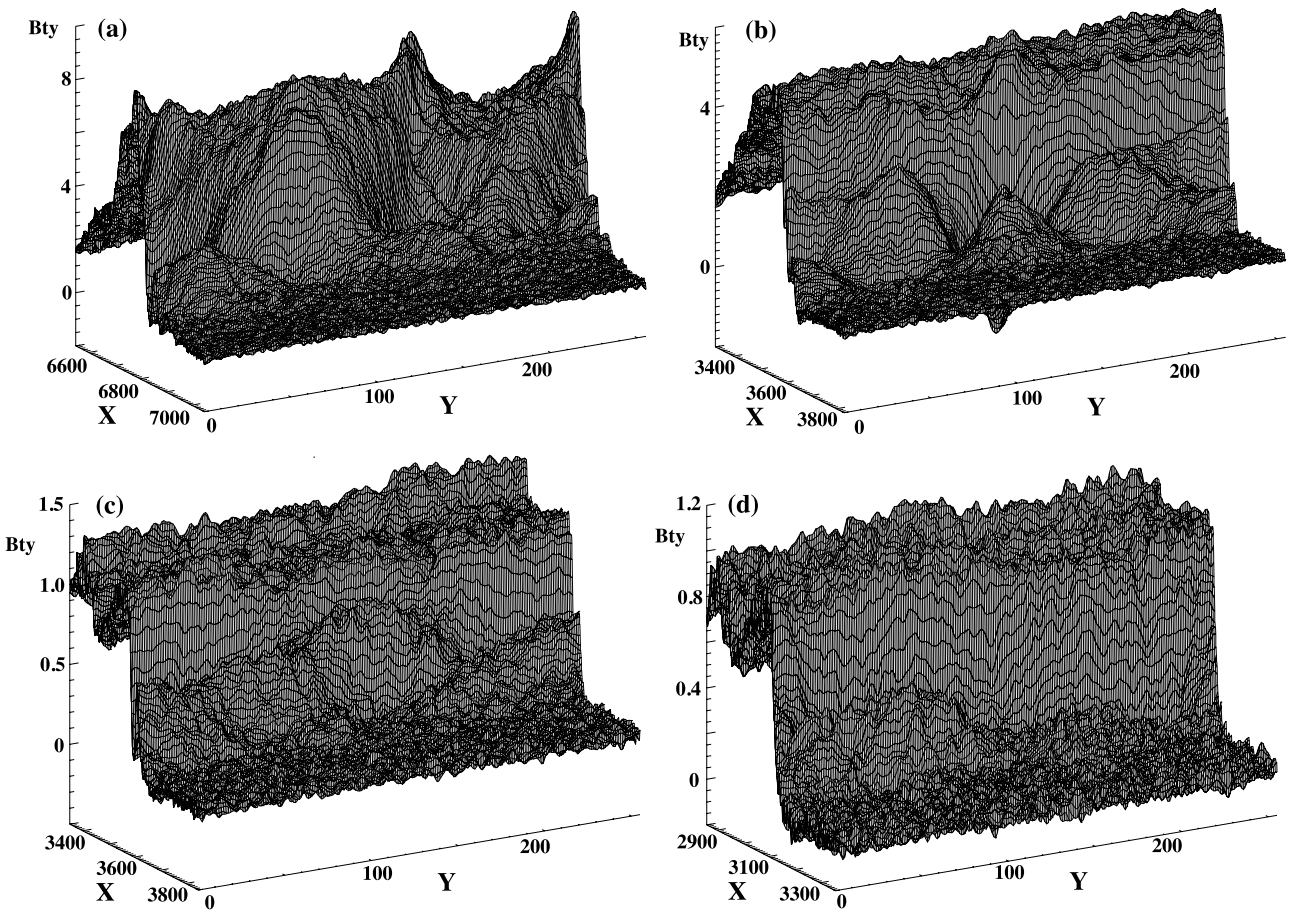

Figure 6. Enlarged three-dimensional view of the main magnetic field component B_{ty} (case 1) at a same given time ($t = 8544\omega_{pe}^{-1}$) corresponding to the four cases of Figure 5 ((a) $M_A = 8.2$, (b) $M_A = 2.54$, (c) $M_A = 1.9$, and (d) $M_A = 1.7$).

persistent self-reformation is evidenced. In contrast, for 2-D PIC simulations, both self-reformation and whistler waves emission can coexist together at any time of a given run, and the self-reformation becomes progressively dominant as M_A decreases.

[25] 3. The impact of the space resolution has been also analyzed and can be summarized as follows. With a high resolution ($\Delta x = 0.05c/\omega_{pi}$), increasing M_A allows for simultaneously triggering the self-reformation and the whistler waves emission. In contrast, when a lower resolution ($\Delta x = 0.1c/\omega_{pi}$) is used (not shown here), the self-reformation still starts at an early time but stops shortly because of the lack of high spatial resolution rather than by the emergence of strong whistler waves emission. This result is confirmed by 1-D hybrid simulations which have been performed in similar conditions (low $M_A = 1.92$) and where the self-reformation disappears too. However, 1-D hybrid simulations performed with the same low $M_A = 1.92$ but with $\Delta x = 0.05c/\omega_{pi}$ exhibit a clear self-reformation. Then, low-M_A shocks analyzed with 2-D hybrid simulations require quite high spatial resolution.

[26] 4. In order to reinforce the importance of 2-D effects several hybrid simulations have been performed with different dimensions L_y of the simulation box with other conditions identical to those of the low-M_A (1.92) shock case. As L_y decreases to a value around $3.2c/\omega_{pi}$ (which is the characteristic $L_{y,w}$ wavelength of the whistler wave), whistler waves are still emitted and no self-reformation occurs. However, when L_y is below $L_{y,w}$ (where $L_y = 1.6c/\omega_{pi}$), no whistler waves are emitted and the self-reformation is recovered. Similar simulations have been performed for 2-D PIC simulations with dimension L_y (64Δ, i.e., almost $1.06c/\omega_{pi}$) of the simulation box (not shown here) lower than the $L_{y,w}$ wavelength of the emitted whistler wave. In this case, a time persistent self-reformation is immediately recovered and no whistler waves are emitted. In summary, both types of simulations performed with a relatively narrow L_y dimension behave as a 1-D simulation.

[27] In contrast with case 1, the self-reformation is well evidenced in case 2 where the static field $\mathbf{B}_0$ is perpendicular to the simulation plane, even for a high Mach number. This same result has been observed for both 2-D PIC and 2-D hybrid simulations (until $M_A = 8.2$ for 2-D PIC and $M_A = 3.2$ for 2-D hybrid simulations). No whistler waves are emitted from the front, and no M_A^{WWE} threshold can be defined in case 2.

4. Comparison With Previous Works

[28] The progressive transition evidenced between both processes as M_A varies (section 3.2 and Figure 1b) allows

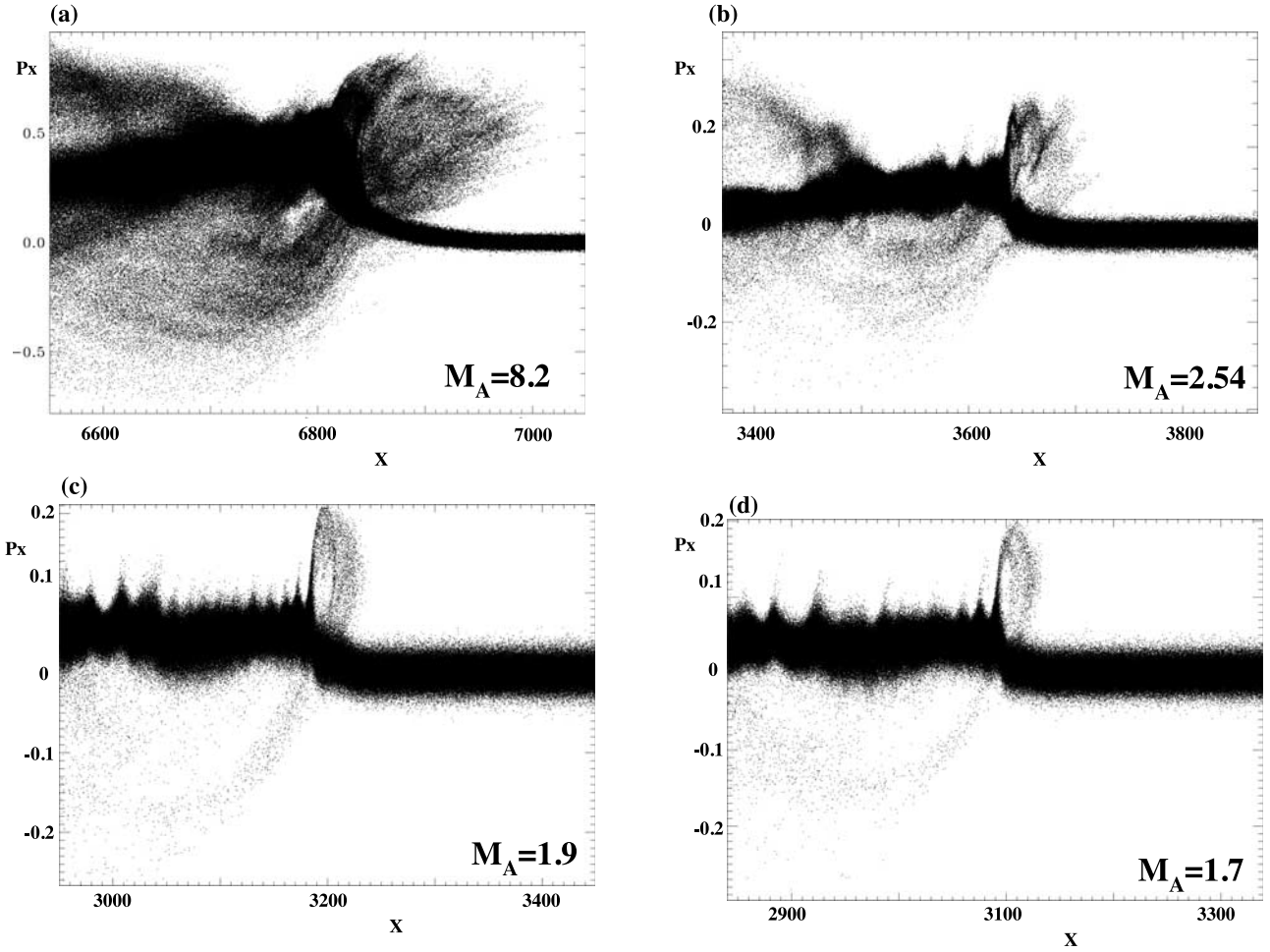

Figure 7. Ion phase space (v_x, x) measured at the same given time $t = 8544\omega_{pe}^{-1}$ as in Figure 6 for the four cases of Figure 5 ((a) $M_A = 8.2$, (b) $M_A = 2.54$, (c) $M_A = 1.9$, and (d) $M_A = 1.7$). Plots are made within a same spatial width $\Delta x = 500$. In order to illustrate more clearly the relative disappearance/occurrence of the ion vortex, the ion phase space is partially y-averaged over a same limited interval $\Delta y = 64$ for all cases.

for clarifying the relationship between present and previous works. In particular, it confirms that results of Paper 1 are not in disagreement with previous results but rather represent particular conditions of parametric plasma and the Mach regime. Even in these conditions, the shock front always presents some nonstationarity (2-D effects) which needs to be defined more carefully. Previous experimental results evidenced the presence of reflected secondary ions, indicating the formation of ion torus in supercritical shock regimes [*Sckopke et al.*, 1983]. Such reflected ion dynamics fits quite well with the features expected from collimated trajectory of reflected ions as observed herein for slow (supercritical) shocks (case 1) and any supercritical shock regime of case 2. However, some of these observations have been obtained for a wide M_A range of supercritical shocks ($M_A = 2-12$) and do not fit with present results in similar conditions of case 1 (i.e., $M_A \geq 1.98$). In fact, a strict comparison cannot be performed at present since the present study is restricted to 2-D perpendicular shocks only. Oblique 2-D quasi-perpendicular shocks are under active investigation, and results will be presented in a separate study. In addition, full 3-D simulations will certainly clarify the relationship between results obtained in cases 1 and 2 and are left for further analysis.

[29] The comparison of present results with previous PIC and hybrid simulation results requires a delicate analysis. For clarity, we will separate it into two parts.

4.1. Comparison With Previous 2-D Full Particle Simulations

[30] Previous 2-D simulations of perpendicular supercritical shocks [*Lembège and Savoini*, 1992] have evidenced self-reformation of the shock front even as the static $\mathbf{B}_0$ field is within the simulation plane, which seems to be in disagreement with the results of Paper 1. This apparent contradiction totally disappears by performing a four-step careful comparative analysis in order to recover the conditions of *Lembège and Savoini* [1992]. First, one has to remember that a much lower mass ratio has been used ($M_i/m_e = 42$ instead of 400 here); second, the Mach regime was lower ($M_A = 3.2$ instead of 4.93 here), and third the L_y dimension of the simulation box was much lower ($L_y = 128$ instead of 256 here). In order to analyze each effect, three separate PIC simulation runs have been performed.

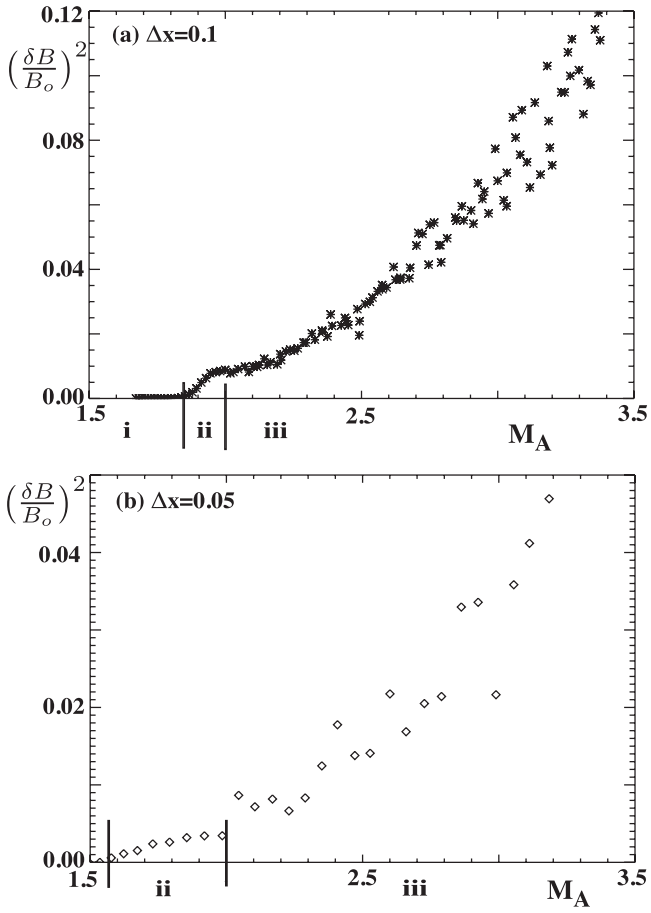

Figure 8. Energy of the whistler waves emitted from the shock front versus Mach number (case 1) for two different spatial resolutions: (a) $\Delta x = 0.1c/\omega_{pi}$ and (b) $\Delta x = 0.05c/\omega_{pi}$. In both cases, $\Delta y = 0.2c/\omega_{pi}$ and resistivity $\eta = 10^{-4}\mu_0 v_A{}^2\omega_{ci}{}^{-1}$. Results are issued from 2-D hybrid simulations: the energy of waves is measured at the same last time ($t = 20\omega_{ci}{}^{-1}$) of each run. All other plasma parameters are unchanged with respect to Table 1. In both cases, interval ii corresponds to the transition regime (see text). The diffusion of points for high M_A is mainly due to the increasing time variability of the emitted whistler waves as M_A increases (see text).

[31] The first run is identical to the reference run used herein (case 1 in Figure 1a) except a lower mass ratio (42 instead of 400) is now used. Surprisingly, the whistler waves emission is still observed over the most part of the run (the full run, not shown here, covers a time range $t = 3456\omega_{pe}^{-1}$, i.e., $40.65\omega_{ci}^{-1}$). One striking feature is that a few clear self-reformations are observed in the y-averaged profile of the magnetic field at an early time and progressively disappear at later times (Figure 10a). Simultaneously, the amplitude of the whistler waves is relatively low at an early time but becomes large enough to dominate the self-reformation at later times. In some ways, one retrieves some features of a transition regime similar to that defined in section 3.2.1 for $M_i/m_e = 400$. The transition between both processes is illustrated in the full 3-D plots of the magnetic field at different times of the same run (Figures 10b and 10c). In contrast, the reference run ($M_i/m_e = 400$) does not show any clear self-reformation at an early time of the run (Figure 10d). Then, two PIC simulations performed in similar Mach regimes ($M_A = 4.58$ in Figures 10a–10c and $M_A = 4.93$ in Figures 10d–10f), but using quite different mass ratios, show again whistler waves emission; these only differ at early times. For a low mass ratio, the nonlinear whistler waves need more time to build up and reach a level high enough to drive the whole dynamics of the shock front. In summary, the use of a low mass ratio does not have drastic consequences in most parts of the run where the whistler waves emission is still dominant.

[32] Second, a new 2-D PIC simulation run has been performed similar to that of Figure 10a but with a lower Mach regime $M_A = 2.1$ (not shown) as in the work by *Lembège and Savoini* [1992] ($M_A = 2.17$). Surprisingly again, nonlinear whistler waves emission is dominant during most of the run. The results are similar to those of Figure 10a: the self-reformation is observed at a very early time but is suppressed progressively at later times. In the present case, the self-reformation persists quite well since whistler waves reach a smaller amplitude for low M_A than for larger M_A.

[33] Third, another 2-D PIC simulation run has been performed similar to the previous one, in which the length L_y of the box has been reduced in order to recover the conditions of *Lembège and Savoini* [1992] ($L_y = 128$ instead of 256 as in our reference run used here). Again, no self-reformation is apparent at the end of the run, which means that using a smaller L_y has no noticeable impact in the present case; L_y is still larger than the excited whistler wavelength for $M_i/m_e = 42$. Also, it is important to remember that the ion inertial length increases with the mass ratio. Then, a sufficient large box along the y axis is necessary to cover at least several ion inertial lengths in order to observe the whistler waves emission.

[34] A more accurate analysis reveals that the time length of the run made by *Lembège and Savoini* [1992] is much shorter than the present one (because of computational constraints at that time). Then, one reaches the fourth step, where the comparison must be focused on comparative times. Namely, the time length of the run made by *Lembège and Savoini* [1992] is from 0 to $864\omega_{pe}^{-1}$ (i.e., $10\omega_{ci}^{-1}$). That time range reported in the present results falls within the range when the self-reformation is still large enough to dominate the shock front dynamics. Then, one recovers the self-reformation as observed by *Lembège and Savoini* [1992] at a comparative time. This four-step process illustrates the deep care for bringing in the comparison with other results. It emphasizes the respective impact of varying the Mach number, the mass ratio, the length L_y, and the time length of the run on the obtained results. Presently, this allows one to explain why whistler waves emission has not been observed in previous 2-D PIC simulations of *Lembège and Savoini* [1992]. Moreover, a too small y dimension of the simulation box may be also invoked in a recent 2-D PIC simulation of *Umeda et al.* [2008] ($L_y = 64$), where whistler waves emission has not been observed.

[35] Additional information may be obtained on the impact of changing the mass ratio on the emitted whistler waves. Results of the space charge effects field are shown in Figure 11 for comparative Mach regimes and at very late

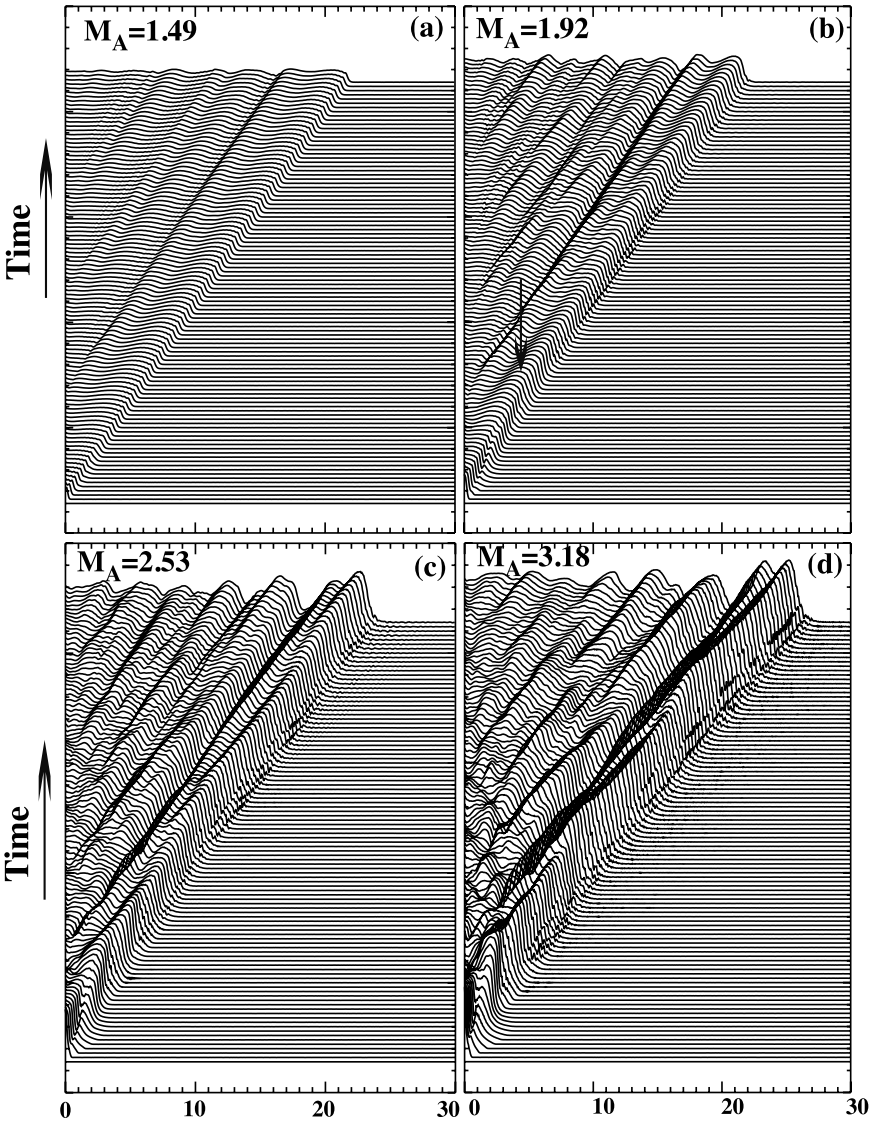

Figure 9. Stack plot of the main magnetic field B_{ty} (case 1) for (a) $M_A = 1.49$, (b) $M_A = 1.92$, (c) $M_A = 2.53$, and (d) $M_A = 3.18$ for the time interval $0 \leq t \leq 20\omega_{ci}^{-1}$. Results issued from 2-D hybrid simulation with $\Delta x = 0.05c/\omega_{pi}$ and resistivity $\eta = 10^{-4}\mu_0 v_A{}^2\omega_{ci}{}^{-1}$. All other parameters are unchanged with respect to Table 1. The time interval between two successive curves is $t = 0.2\omega_{ci}{}^{-1}$.

times of each simulation when whistler waves are dominating the shock front dynamics ($t = 10.68\omega_{ci}^{-1}$ for Figure 11a, and $t = 40.65\omega_{ci}^{-1}$ for Figure 11b). Surprisingly, the maximum amplitude of the (y-averaged) electrostatic field E_{lx} is almost unchanged for different mass ratios and is around 0.6. When a higher mass ratio and a relatively high space resolution are used, a more accurate analysis evidences two points: (1) steeper profiles of fields are obtained (rather than their amplitudes being changed), and consequently (2) more spiky whistler waves occur in the y-averaged profiles (Figure 11).

4.2. Comparison With Previous 2-D Hybrid Simulations

[36] The absence of whistler waves emission in previous 2-D hybrid simulations may be explained in terms of inappropriate numerical conditions rather than large differences in plasma conditions. Two parameters play a crucial role: the spatial resolution and the phenomenological resistivity η. Previous hybrid simulations [*Hellinger et al.*, 2002] have clearly evidenced that a high-enough spatial resolution is necessary to initiate shock front self-reformation. Namely, self-reformation was observed for space grid $\Delta x \leq 0.2c/\omega_{pi}$, but it is not observed for $\Delta x = 0.5-1c/\omega_{pi}$. This is the main reason why the self-reformation has not been observed during many years since early hybrid simulations of *Leroy et al.* [1981, 1982], where the $\Delta x = 0.5-1c/\omega_{pi}$ value was commonly used. In such cases, the shock ramp could not access a smaller spatial scale which restricts the ramp steepening in most other works. More precisely, *Leroy et al.* [1982] have only observed a time modulation of the magnetic field overshoot amplitude (cyclic time of the order of the ion gyroperiod), which should not be confused with the present so-called "shock front self-reformation," including both time variations of the overshoot/foot ampli-

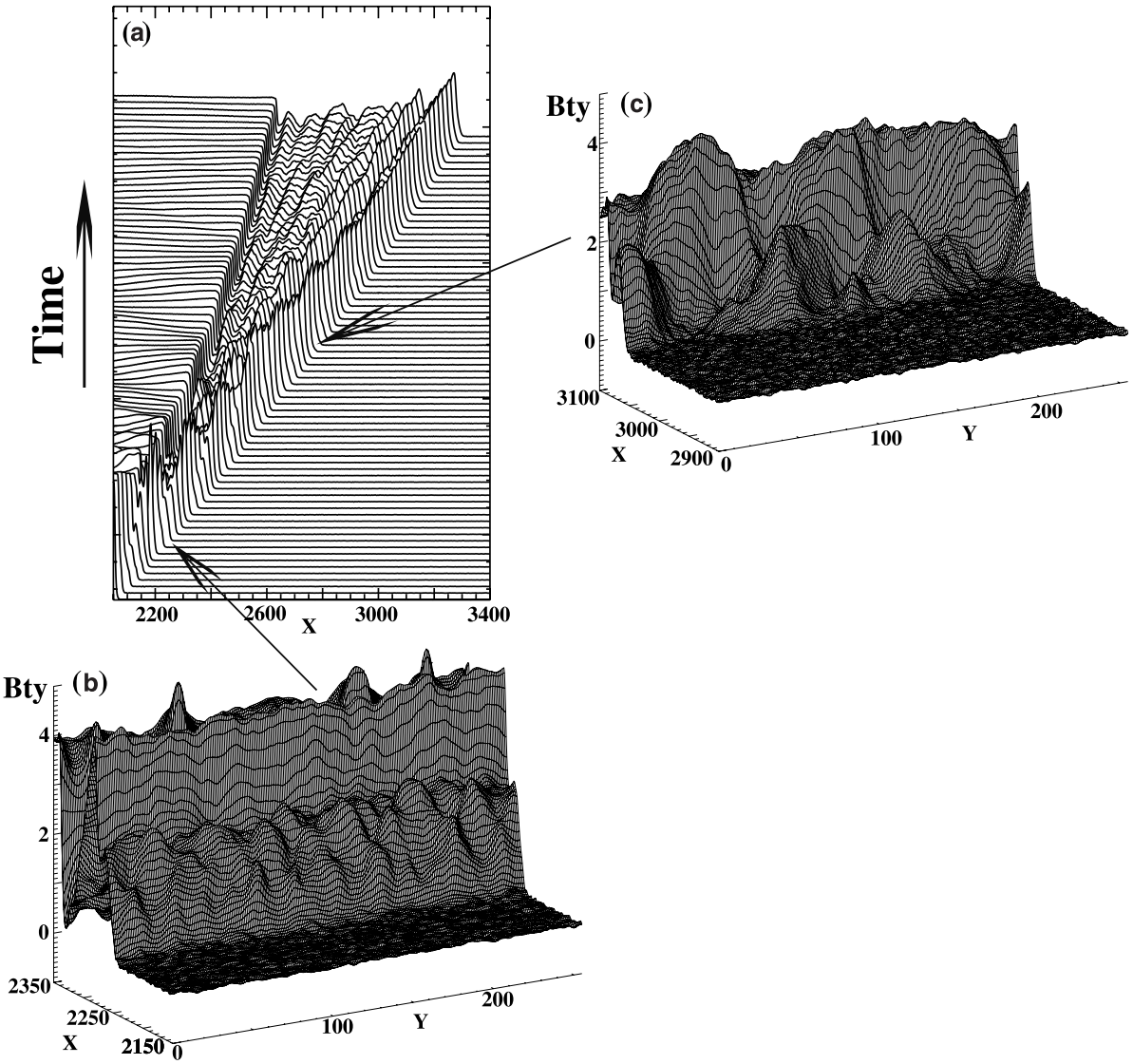

Figure 10. Figures 10a–10c show results obtained for mass ratio $M_i/m_e = 42$ as $B_0 = B_{0y}$ (case 1). The Mach regime ($M_A = 4.58$) is approaching that used for the reference run ($M_A = 4.93$ in Figure 1, case 1). (a) Enlarged view of the stack plot of the y-averaged B_{ty} component at early times of the run within the time range $t = 24–1728\omega_{pe}^{-1}$ ($0.3–21\omega_{ci}^{-1}$) and of the 3-D profiles of the main magnetic field B_{ty} at two different times (b) $t = 240\omega_{pe}^{-1}$ and (c) $t = 1560\omega_{pe}^{-1}$. Figures 10d–10f show similar results for the reference run ($M_i/m_e = 400$ as $B_0 = B_{0y}$ (same reference run as Figure 1a, case 1). (d) Same as Figure 10a except within the time interval $t = 48–3792\omega_{pe}^{-1}$ ($0.6–4.75\omega_{ci}^{-1}$) and same as Figures 10c and 10d except measured at two different times: (e) $t = 672\omega_{pe}^{-1}$ and (f) $t = 2736\omega_{pe}^{-1}$.

tude and the spatial width of the ramp/foot as seen in Figure 1 (also *Savoini et al.* [2005, Figure 1], for instance). One exception holds for very high Mach number shocks [*Quest*, 1985], where the self-reformation has been observed. In the present case of moderate Mach number ($M_A = 3–4$), the spatial resolution has been chosen to be high enough ($\Delta_x = 0.1c/\omega_{pi}$) to allow a strong ramp steepening to set up, which initiates both the shock front self-reformation and the whistler waves emission (section 2).

[37] The second point is concerning the impact of the resistivity η commonly used in hybrid simulations. The difficulty is that increasing η leads to a decrease of the ramp steepening which has an impact on both processes. How to separate both? The answer is obtained by remembering that the self-reformation is basically a 1-D effect (also retrieved in 2-D simulation), while whistler waves emission is strictly a 2-D effect. In order to separate both effects, one must first perform 1-D hybrid simulations, in which one measures the maximum strength of the main magnetic field gradient at the shock ramp for different resistivity values ($\eta = 10^{-4} – 10^{-2}\ \mu_0 v_A^2 \omega_{ci}^{-1}$). A spatial resolution $\Delta x = 0.1c/\omega_{pi}$ is fixed for all of these simulations. All other plasma and numerical parameters are unchanged with respect to the values in Table 1. A weak difference is measured in Mach number regimes ($M_A = 2.11–2.05$) from $\eta = 10^{-4}\mu_0\ v_A^2\omega_{ci}^{-1}$ to $\eta = 10^{-2}\ \mu_0\ v_A^2\ \omega_{ci}^{-1}$. Results are reported in Figures 12 and 13.

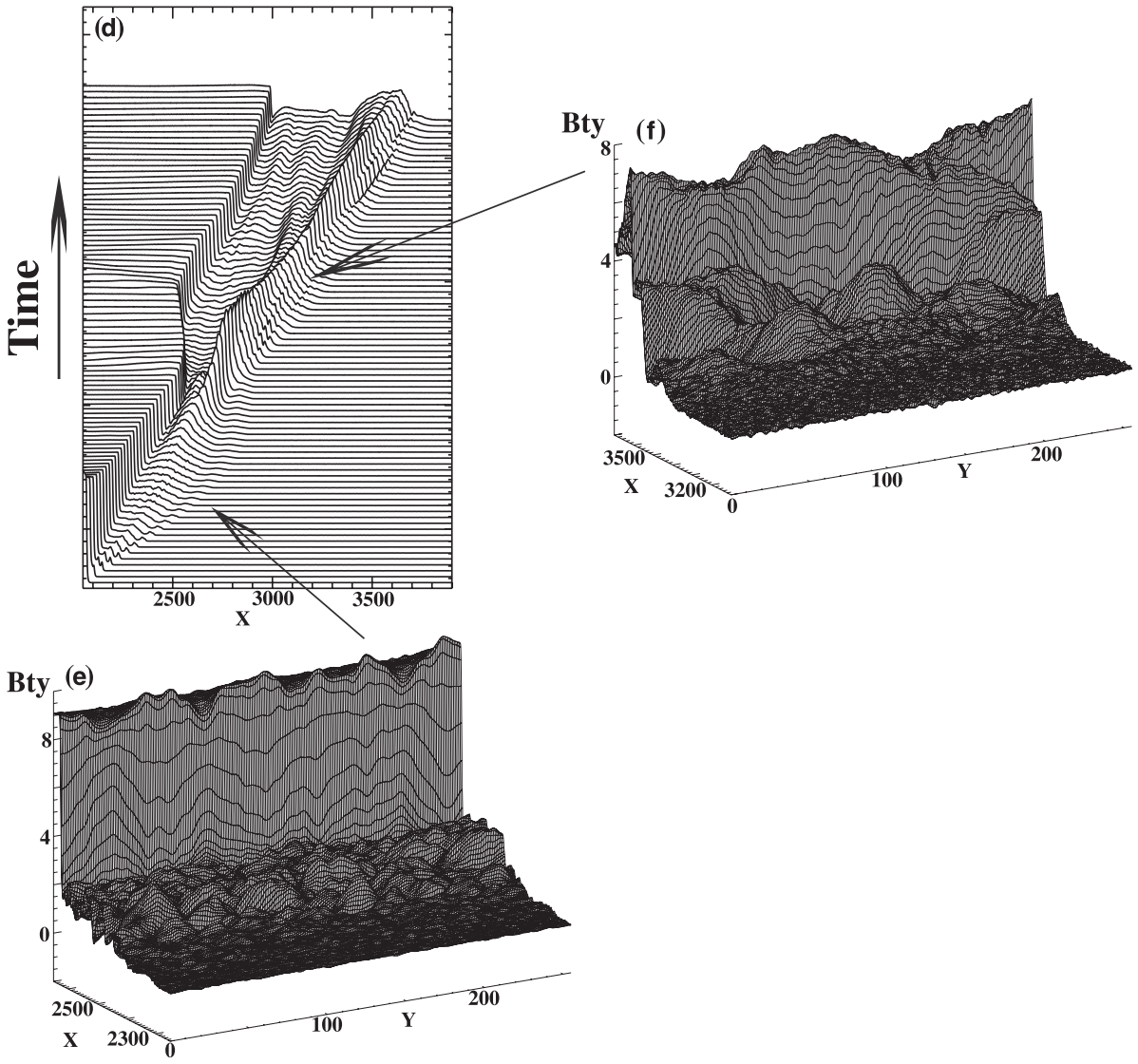

Figure 10. (continued)

For the low-resistivity run ($\eta = 10^{-4}\mu_0 v_A^2 \omega_{ci}^{-1}$), a "partial" self-reformation is observed while it totally disappears for the high-resistivity run ($\eta = 10^{-2}\mu_0 v_A^2 \omega_{ci}^{-1}$) where shock front is stationary, as shown in Figures 13a–13c. In Figure 13c, only a local minimum B_{ty} field is observed in the foot. Figure 12 can be used as a reference curve where two regimes can be defined. First, the shock front is stationary for high-resistivity values, i.e., as the maximum value of the B_y gradient is around 8–10. This is illustrated in stack plots of Figure 13c for $\eta = 10^{-2}\mu_0 v_A^2 \omega_{ci}^{-1}$. A clear ramp and a foot are evidenced, but the steepening of the ramp is restricted by the high η value and cannot initiate a self-reformation even if the spatial resolution is relatively high. Second, a partial self-reformation is observed for lower resistivity, i.e., herein as the maximum value of the B_{ty} gradient is around 11–15 (Figure 12). This is illustrated in Figure 13b for $\eta = 1.58 \times 10^{-3}\mu_0 v_A^2 \omega_{ci}^{-1}$. The self-reformation is partial in the sense that the foot amplitude is increasing but stays relatively weak and never reaches an amplitude comparable to that of the old ramp. Instead, the new ramp crashes down and restarts reflecting new incoming ions. As a consequence, the old ramp seems unaffected; the ramp and foot seem to behave independently of each other. Then, the old ramp looks almost stationary, while the foot only shows some amplitude modulation with a cyclic period of 0.45 τ_{ci} and 0.49τ_{ci} shown in Figures 13a and 13b, respectively, but its width is almost unchanged (in contrast with a full self-reformation). If the resistivity continues to decrease ($\eta = 10^{-4}\mu_0 v_A^2 \omega_{ci}^{-1}$ in Figure 13a), the self-reformation is more clearly evidenced since the foot reaches an amplitude comparable to that of the old ramp and starts reflecting new incoming ions. Again, the new ramp crashes down just after reaching its maximum amplitude. In contrast with the previous case, the new set of freshly reflected ions continues to build up a new foot. As a consequence, the original ramp is almost unchanged since the newly formed ramp always crashes down. In this sense, we can consider that the self-reformation is still partial. Extended parametric analysis (results not shown here) indicates that the full self-reformation is still not recovered even with a null resistivity ($\eta = 0$). Then, one has to face the difficulty of performing more expensive 1-D/2-D hybrid simulations with much

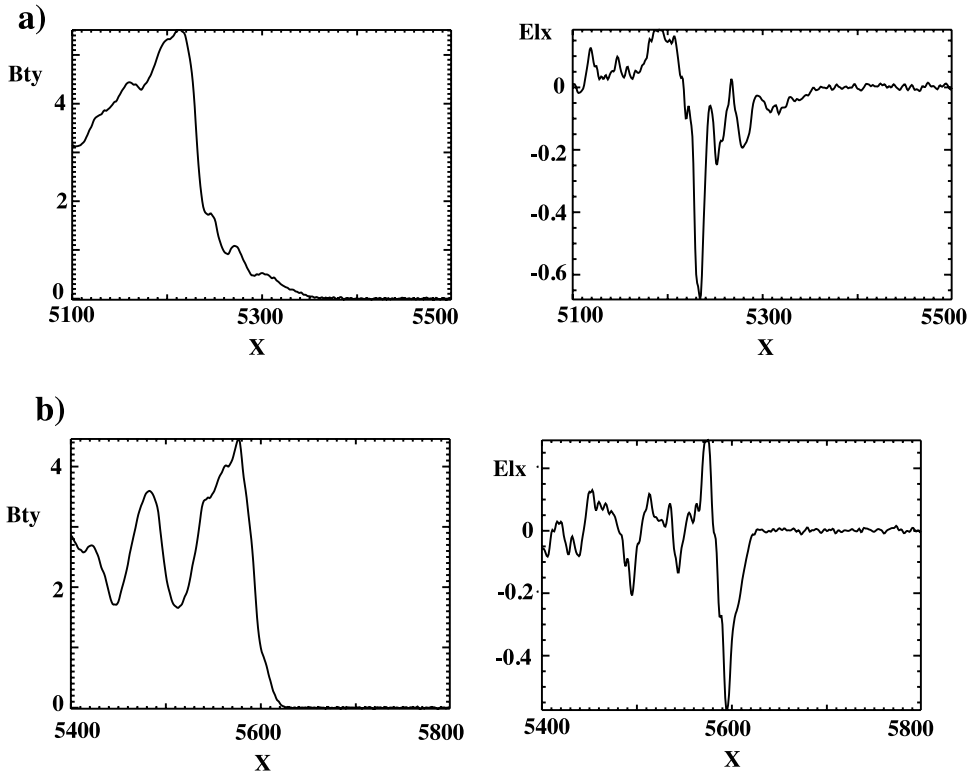

Figure 11. Comparison of the y-averaged electrostatic field E_{lx} obtained for different mass ratios as $B_0 = B_{0y}$ (case 1): (a) $M_i/m_e = 400$ and $M_A = 4.93$ and (b) $M_i/m_e = 42$ and $M_A = 4.58$. Results are issued from 2-D PIC simulation.

higher spatial resolution. The use of such conditions of hybrid simulations can be questionable in terms of computing costs when compared to 1-D/2-D PIC simulations performed with a reasonable mass ratio. In summary, these results illustrate the strong impact of both the spatial resolution and the resistivity values on the shock dynamics in hybrid simulations.

[38] Let us note that the question of accessibility to a small scale (lower than ion scale) is expressed differently in PIC and hybrid simulations. In PIC simulations, the accessibility to both ion and electron scales is automatically and self-consistently included because of the use of finite mass ratio. However, using a more or less realistic mass ratio value allows for controlling the steepening strength (section 4.1). Of course, higher mass ratio allows for an easier separation between ion and electron scales but requires computer capacities relatively large, in particular for 2-D simulations. In hybrid simulations, the accessibility to a small scale is controlled by the $\Delta x/(c/\omega_{pi})$ ratio, but the strength of the ramp steepening is controlled by both the $\Delta x/(c/\omega_{pi})$ ratio and the resistivity values. The present study shows that using a high resistivity value and a low spatial resolution will stop almost simultaneously the self-reformation and the emission of nonlinear whistler waves.

[39] Let us specify that these nonlinear whistler waves should not be confused with front ripples, larger-scale ones related to Alfvén ion cyclotron and/or mirror waves or shorter ones related to lower hybrid waves.

[40] 1. Alfvén ion cyclotron (and/or mirror) waves are excited by the ion temperature anisotropy [*Winske and Quest*, 1988], but their linear growth takes place over a much longer time and for larger M_A [*Hellinger and Mangeney*, 1997], as compared to the short occurrence time of the nonlinear whistler waves. Analysis by *Lowe and Burgess* [2003] shows that these ripples have features different from the present nonlinear whistler waves: (1) these ripples propagate in the shock rest frame along the front with a phase velocity of the order of the local Alfvén velocity and (2) the amplitude of the rippling reaches a maximum at the overshoot (and not within the foot). It is important to note that a relation of these shock ripples to the self-reformation process is an open question. The high spatial $\Delta x = \Delta y = 0.2$ resolution used by *Lowe and Burgess*

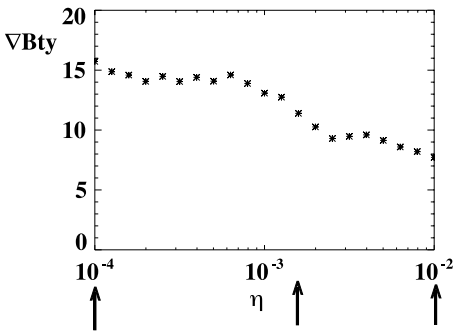

Figure 12. Maximum value of main magnetic field gradient (for B_{ty}) measured at the shock ramp for different resistivity values η. Results are issued from 1-D hybrid simulation runs.

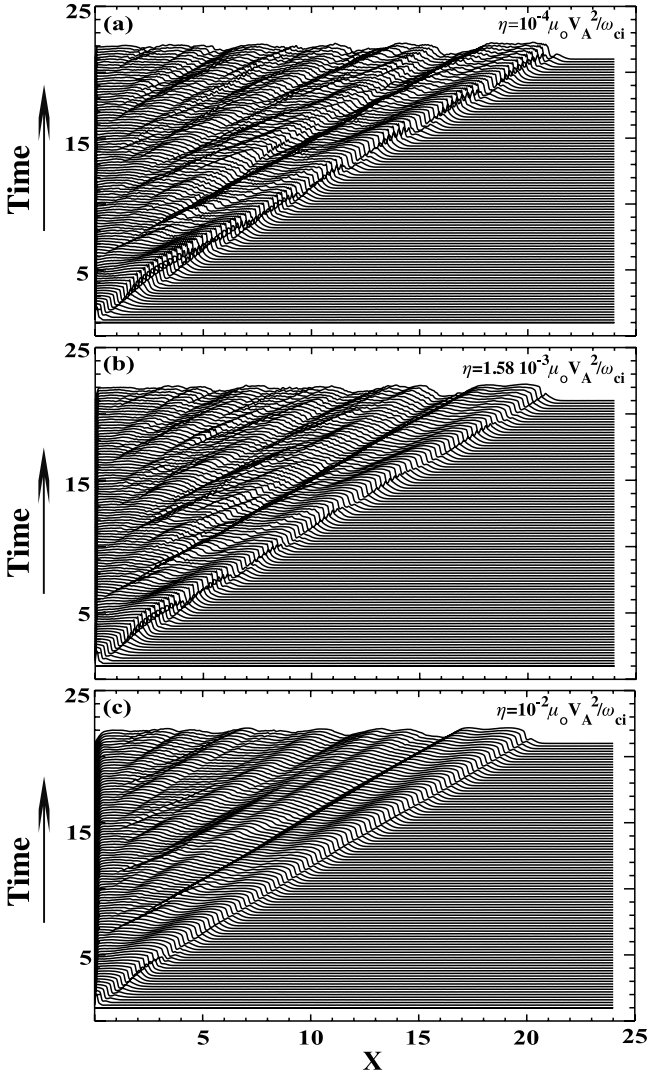

Figure 13. Stack plots of the y-averaged magnetic field obtained for (a) $\eta = 10^{-4}\mu_0 {v_A}^2 {\omega_{ci}}^{-1}$, (b) $\eta = 0.00158\mu_0 {v_A}^2 {\omega_{ci}}^{-1}$, and (c) $\eta = 10^{-2}\mu_0 {v_A}^2 {\omega_{ci}}^{-1}$. Here $\beta_e = 0.24$ and $\beta_i = 0.15$; $M_A = 2.11$ (for $\eta = 10^{-4}\mu_0 {v_A}^2 {\omega_{ci}}^{-1}$) decreases to 2.05 (for $\eta = 10^{-2}\mu_0 {v_A}^2 {\omega_{ci}}^{-1}$). The three cases (Figures 13a–13c) are indicated by arrows in Figure 12. The measured period of the partial self-reformation is 0.45 τ_{ci} (Figure 13a) and 0.49τ_{ci} (Figure 13b), where τ_{ci} is the ion upstream gyroperiod.

[2003] could allow for evidencing the nonlinear whistler waves when $\mathbf{B}_0$ is inside the simulation plane and the self-reformation as $\mathbf{B}_0$ is outside the simulation plane. However, neither of these processes have been mentioned; here we just note that *Lowe and Burgess* [2003, Figure 3] indicate a presence of short-wavelength waves slowly propagating in the shock rest frame. These waves may be related to the nonlinear whistlers. Unfortunately, the lack of information concerning the resistivity used in the paper does not allow for estimating whether the two processes are not affected by a too high resistivity. Moreover, an extensive work to oblique propagating shocks is necessary to clarify whether the present nonlinear whistler waves are related or not to the wave activity observed by *Lowe and Burgess* [2003].

[41] 2. The lower–hybrid frequency waves (LHF) are excited by cross-field current instabilities as observed in the shock front when $\mathbf{B}_0$ is outside the simulation plane (Figure 2a, case 2). Indeed, these LHF waves require the cross-field currents to lie within the simulation plane as in case 2 only. In addition, these LHF waves are observed in 2-D PIC simulations and not in 2-D hybrid simulations (Figure 3, case 2) where the LHF range is not accessible. This is in contrast with the nonlinear whistler waves observed both in 2-D PIC and 2-D hybrid simulations.

5. Conclusions

[42] The present results represent an extension of a previous work (Paper 1), where both 2-D hybrid and 2-D PIC simulations have evidenced that under some plasma conditions and supercritical shock regimes the front of a perpendicular shock can be quasi-stationary: large-amplitude whistler waves are emitted from the front, and the shock front self-reformation (mainly driven by the accumulation of reflected ions) is inhibited. This result could seem to be in disagreement with previous results where the shock front is expected to be nonstationary (self-reformation). The present analysis clarifies the situation and shows that this apparent contradiction disappears for the following reasons.

[43] First, the quasi-stationary behavior needs to be defined more accurately. The time variability of the shock front controlled by the whistler waves emission appears to be less pronounced than that due to the self-reformation, when considering a time range covering one or several ion gyroperiods. In addition, the whistler waves emission is essentially a 2-D process, while the self-reformation is mainly a 1-D process. The time variability of such a 2-D process is strongly smoothed out when y averaging 2-D profiles and appears much less spectacular in an "artificial" 1-D representation.

[44] Second, for a fixed β_i value, the WWE persists for high M_A, particularly as long as M_A is above a certain threshold M_A^{WWE}. The dissipation associated with the accumulation of reflected ions is not strong enough to balance alone the nonlinear effects (ramp steepening). In contrast, for low (but still supercritical) M_A below this critical threshold M_A^{WWE}, the dissipation effects brought by ion reflection are dominant. The self-reformation is fully retrieved, and the amplitude of the whistler waves is negligible.

[45] Third, there exists a transition regime in a Mach number around the critical value M_A^{WWE} within which both processes can coexist together (whistler waves emission is embedded within the self-reformation). For a run performed within this transition regime, the self-reformation starts first and drives the whole shock dynamics at early times of the run. Simultaneously, whistler waves emission also starts but still has a low amplitude for low M_A. As M_A increases, these nonlinear whistler waves reach an amplitude high enough to drive the shock dynamics. The competition between both processes can be expressed in terms of time for the self-reformation to establish (a portion of upstream ion gyroperiod) versus the time for the nonlinear whistler wave to grow and reach an amplitude high enough to diffuse noticeably the reflected ions and to destroy their coherent motion (a

condition necessary for the self-reformation to establish). For M_A above the transition regime, nonlinear whistler waves are emitted at an early time, even before the self-reformation can be initiated. Both processes contribute to the shock front nonstationarity but with different signatures.

[46] Fourth, some differences are observed between 2-D PIC and 2-D hybrid simulations concerning the coexistence of both processes within the transition regime and can be summarized as follows.

[47] 1. In 2-D hybrid simulations, the competition between the two processes is observed in time within a same run (as described above) with a sequential occurrence (self-reformation at early times and waves emission at later times). However, it is particularly difficult to observe a time-persistent full self-reformation for low M_A, even in optimal conditions of very low resistivity and high spatial resolution. Then, the absence of whistler waves emission at low M_A is not associated closely with the recovery of the self-reformation.

[48] 2. In contrast, in 2-D PIC simulations based on a high mass ratio (400 herein), the coexistence of both processes persists quite well within the whole time length of the same run. In this case, 2-D PIC results differ from those issued from 2-D hybrid simulations, and the disappearance of whistler waves emission at low M_A can be associated with the full recovery of the self-reformation. When a weak mass ratio (42) is used, results are similar to 2-D hybrid simulation results (sequential occurrence).

[49] Fifth, nonlinear whistler waves are observed for a strictly perpendicular shock, as $\mathbf{B}_0$ is within the simulation plane. In contrast, as $\mathbf{B}_0$ is perpendicular to the simulation plane, no whistler waves emission is evidenced even for a large Mach number, and only self-reformation is observed and drives the whole shock front dynamics. The access to obliquity appears to be a condition for the whistler waves to occur.

[50] Sixth, a deeper investigation based on several parametric analyses has allowed for explaining why nonlinear whistler waves have not been observed in previous simulations. Present results issued from 2-D PIC and 2-D hybrid simulations mainly depend on the M_A value, the size L_y of the simulation box along the shock front, and the time length of the simulation as M_A decreases. However, some specific features occur for each simulation code.

[51] 1. The main results of 2-D PIC simulations are mainly controlled by the M_A variation. The variation of the mass ratio has only an impact on the spiky features of the macroscopic fields (at the ramp) and of the emitted whistler waves (in the foot) for high M_A. It has also some impact on the relative time persistence of the self-reformation within the transition regime.

[52] 2. Moreover, 2-D hybrid simulation results are strongly dependent both on the resistivity value and on the spatial resolution, whatever the M_A regime is.

[53] The transition between the two configurations of $\mathbf{B}_0$ will require the use of 3-D PIC and/or 3-D hybrid simulations where any orientation of the static $\mathbf{B}_0$ field is allowed. Moreover, the comparison with experimental results will certainly require extending the study to oblique quasi-perpendicular shocks for which most experimental satellite data have been obtained. A direct comparison between experimental and simulation results presently obtained for a strictly perpendicular shock is not possible yet.

[54] **Acknowledgments.** This paper has been written while one of the authors (B.L.) was a visiting professor at Research Institute for Sustainable Humanosphere of Kyoto University, which is deeply thanked for the welcome and hospitality. P.H. and P.M.T. acknowledge the Czech grants GAAV IAA300420702 and IAA300420602. The hybrid simulations have been performed on the Amalka supercomputing facility at IAP, AS CR. B.L. and P.S. thank IDRIS computer center (Orsay), where full particle PIC simulations have been performed.

[55] Amitava Bhattacharjee thanks Takayuki Umeda and another reviewer for their assistance in evaluating this paper.

References

Biskamp, B., and H. Welter (1972), Numerical studies of magnetosonic collisionless shock waves, *Nucl. Fusion*, *12*, 663–666.

Forslund, D. W., K. B. Quest, J. U. Brackbill, and K. Lee (1984), Collisionless dissipation in quasi-perpendicular shocks, *J. Geophys. Res.*, *89*, 2142–2150.

Hada, T., M. Onishi, B. Lembège, and P. Savoini (2003), Shock front nonstationarity of supercritical perpendicular shocks, *J. Geophys. Res.*, *108*(A6), 1233, doi:10.1029/2002JA009339.

Hellinger, P. (2003), Structure and stationarity of quasi-perpendicular shocks: Numerical simulations, *Planet. Space Sci.*, *51*, 649–657.

Hellinger, P., and A. Mangeney (1997), Upstream whistlers generated by protons reflected from a quasi-perpendicular shock, *J. Geophys. Res.*, *102*, 9809–9819.

Hellinger, P., P. Trávníček, and H. Matsumoto (2002), Reformation of perpendicular shocks: Hybrid simulations, *Geophys. Res. Lett.*, *29*(24), 2234, doi:10.1029/2002GL015915.

Hellinger, P., P. Trávníček, B. Lembège, and P. Savoini (2007), Emission of nonlinear whistler waves at the front of perpendicular supercritical shocks: Hybrid versus full particle simulations, *Geophys. Res. Lett.*, *34*, L14109, doi:10.1029/2007GL030239.

Lee, R. E., S. C. Chapman, and R. O. Dendy (2004), Numerical simulations of local shock reformation and ion acceleration in supernova remnants, *Astrophys. J.*, *604*, 187–195.

Lembège, B., and J. M. Dawson (1987), Self-consistent study of a perpendicular collisionless and nonresistive shock, *Phys. Fluids*, *30*, 1767–1788.

Lembège, B., and P. Savoini (1992), Non-stationarity of a 2-D quasi-perpendicular supercritical collisionless shock by self-reformation, *Phys. Fluids*, *4*, 3533–3548.

Lembège, B., and P. Savoini (2002), Formation of reflected electron bursts by the nonstationarity and nonuniformity of a collisionless shock front, *J. Geophys. Res.*, *107*(A3), 1037, doi:10.1029/2001JA900128.

Lembège, B., J. Giacalone, M. Scholer, T. Hada, H. Hoshino, V. Krasnoselskikh, H. Kucharek, P. Savoini, and T. Terasawa (2004), Selected problems in collisionless-shock physics, *Space Sci. Rev.*, *110*, 161–226.

Leroy, M. M., C. C. Goodrich, D. Winske, C. S. Wu, and K. Papadopoulos (1981), Simulation of a perpendicular bow shock, *Geophys. Res. Lett.*, *8*, 1269–1272.

Leroy, M. M., D. Winske, C. C. Goodrich, C. S. Wu, and K. Papadopoulos (1982), The structure of perpendicular bow shocks, *J. Geophys. Res.*, *87*, 5081–5094.

Lowe, R. E., and D. Burgess (2003), The properties and causes of rippling in quasi-perpendicular collisionless shock fronts, *Ann. Geophys.*, *21*, 1–9.

Quest, K. B. (1985), Simulations of high–Mach-number collisionless perpendicular shocks in astrophysical plasmas, *Phys. Rev. Lett.*, *54*, 1872–1874.

Savoini, P., B. Lembège, V. Krasnosselskhik, and Y. Kuramitsu (2005), Under and over-adiabatic electrons through a perpendicular collisionless shock: Theory versus simulations, *Ann. Geophys.*, *23*, 3685–3698.

Schmitz, H., S. C. Chapman, and R. O. Dendy (2002), The influence of electron temperature and magnetic field strength on cosmic-ray injection in high Mach number shocks, *Astrophys. J.*, *570*, 637–646.

Scholer, M., and S. Matsukiyo (2004), Nonstationarity of quasi-perpendicular shocks: A comparison of full particle simulations with different ion to electron mass ratio, *Ann. Geophys.*, *22*, 2345–2353.

Scholer, M., I. Shinohara, and S. Matsukiyo (2003), Quasi-perpendicular shocks: Length scale of the cross-shock potential, shock reformation, and implication for shock surfing, *J. Geophys. Res.*, *108*(A1), 1014, doi:10.1029/2002JA009515.

Sckopke, N., G. Paschmann, S. J. Bame, J. T. Gosling, and C. T. Russell (1983), Evolution of ion distribution across the nearly perpendicular bow shock: Specularly and non-specularly reflected-gyrating ions, *J. Geophys. Res.*, *88*, 6121–6136.

Umeda, T., Y. Yamao, and R. Yamazaki (2008), Two-dimensional full particle simulation of perpendicular collisionless shock with a shock-rest-frame model, *Astrophys. J.*, *681*, 85–88.

Winske, D., and K. B. Quest (1988), Magnetic field and density fluctuations at perpendicular supercritical shocks, *J. Geophys. Res.*, *93*, 9681–9693.

P. Hellinger and P. M. Trávníček, IAP, AS CR, Bocni II/1401, Prague 141 31, Czech Republic. (petr.hellinger@ufa.cas.cz; trav@ufa.cas.cz)

B. Lembège and P. Savoini, CETP, UVSQ, IPSL, CNRS, 10-12 Avenue de l'Europe, F-78140 Velizy, France. (bertrand.lembege@cetp.ispl.fr; philippe.savoini@cetp.ispl.fr)